



Master's Thesis

Identification of the self regulating effect of power systems using dynamic power system states

to obtain the degree
Master of Science (Diplom Ingenieur)
at the Institute of Energy Systems and Electrical Drives, E370
at the TU Wien in Vienna

under supervision of

Univ.-Prof. Dr.-Ing. Wolfgang Gawlik

and

Dipl.-Ing. Alexander Stimmer
Ing. Martin Lenz, MSc

by

Elias Obererlacher, BSc

Mat.-Nr.: 01335410

Vienna, February 2022

Abstract

The inertia of power systems reduces as conventional power plants are increasingly replaced by renewable, power electronics interfaced generation. In addition, more uncontrolled loads (e.g. asynchronous motors) are being replaced by drives with frequency converters, resulting in a lower self regulating effect (SRE). These reductions lead to several challenges in power system operation and make power systems more prone to frequency instabilities.

This thesis questions the established planning values for the SRE of 1-2 %/Hz and investigates the necessity for adjustment. Furthermore, patterns or correlations of the effect with prevailing conditions are investigated to improve the predictability.

Data from frequency events caused by power imbalances larger than 1 GW were collected and processed. A top-down approach with three different methods is used to identify the SRE and the composition of the power system frequency characteristic (K-factor).

The RoCoF zero crossing method and the fixed supporting points method can be considered as simple identification approaches, however, they tend to provide implausible SRE values in some cases. The optimal fit method appears to be more robust and suitable to estimate the SRE.

Based on statistical analysis a SRE larger than 1 %/Hz can be confirmed. Furthermore, no decrease of the SRE within the analyzed time interval of the events was found. Moreover, no patterns or correlations of the SRE with season, day of the week and time of the day has been identified.

Within this thesis it has also been shown that the overall K-factor is typically higher compared to the Design Hypothesis of the Continental European (CE) power system. This can be explained by an over-fulfillment of the Frequency Containment Reserve (FCR) and a potentially higher SRE and confirms that the Design Hypothesis serves well as a worst case assumption.

The decomposition of the K-factor depends on the dynamics of the main influencing components. The simple dynamics approach used may not perfectly match the complex response mechanism and may need to be adjusted for further studies. In conclusion, there is a strong need for accurate monitoring of FCR activation to determine the SRE more precisely.

Kurzfassung

Die Trägheit des Stromnetzes nimmt mit zunehmendem Ersatz konventioneller Kraftwerke durch erneuerbare, umrichterbasierte Erzeugungsanlagen ab. Zusätzlich werden vermehrt unregelmäßige Lasten (z.B. Asynchronmotoren) durch Antriebe mit Frequenzumrichtern ersetzt, was zu einer Verringerung des Selbstregelleffekts (SRE) führt. Diese Änderungen stellen große Herausforderungen für den Netzbetrieb dar und begünstigen die Anfälligkeit des Stromnetzes auf Frequenzinstabilitäten.

In dieser Arbeit sollen die etablierten Planungswerte für den SRE von 1-2 %/Hz hinterfragt und die Notwendigkeit einer Anpassung untersucht werden. Darüber hinaus werden Muster oder Korrelation des SRE mit den vorherrschenden netzbetrieblichen Rahmenbedingungen untersucht, um die Vorhersagbarkeit des SRE für zukünftige Systemstudien zu verbessern.

Für diesen Zweck wurden Daten von Frequenzereignissen, verursacht durch Leistungsungleichgewicht größer als 1 GW, gesammelt und aufbereitet. Ein Top-Down-Ansatz mit drei unterschiedlichen Methoden wird verwendet, um den SRE und die Zusammensetzung der Leistungs-Frequenz Charakteristik des Netzes (K-Faktor) zu ermitteln.

Die „RoCoF-Nulldurchgangsmethode“ und die „Fixe-Stützstellen-Methode“ liefern trotz ihrer einfachen Konzeption tendenziell unplausible Werte. Die „Optimierungsmethode“ weist verglichen zu den anderen Methoden eine erhöhte Robustheit und bessere Eignung zur Bestimmung des SRE auf.

Mittels einer statistischen Analyse kann ein SRE größer als 1 %/Hz bestätigt werden. Des Weiteren wurde keine Abnahme des Selbstregelleffekts innerhalb des untersuchten Zeitbereichs festgestellt. Ebenso wurde kein Muster oder Korrelation des Effekts mit der Jahreszeit, dem Wochentag oder der Tageszeit entdeckt.

Im Rahmen dieser Arbeit wird auch gezeigt, dass der K-Faktor typischerweise größer ist als in der Design Hypothese des kontinentaleuropäischen (CE) Verbundnetzes. Dies lässt sich durch eine Übererfüllung der Primärregelreserve und eines potenziell höheren Selbstregelleffekts erklären und bestätigt somit die Design Hypothese als Worst-Case-Annahme.

Die Komposition des K-Faktors hängt stark von der Dynamik der wichtigsten beeinflussenden Komponenten ab. Mit dem vereinfachten dynamischen Ansatz kann der komplexe Reaktionsmechanismus eines Verbundnetzes möglicherweise nicht perfekt abgebildet werden. Für zukünftige Studien wird empfohlen die Dynamik des Selbstregelleffekts und der Primärregelreserve gegebenenfalls anzupassen. Abschließend bekräftigen diese Erkenntnisse ebenfalls den Bedarf einer genaueren und kontinuierlichen Überwachung der Primärregelreserven, um den SRE genauer zu bestimmen.

Table of contents

1	Introduction.....	1
1.1	Background and motivation	1
1.2	Major objective of the thesis and applied method.....	2
1.3	Structure of the thesis	2
2	Theory.....	3
2.1	Frequency response of synchronous machines.....	4
2.2	Inertia constant of the network	7
2.3	Self regulating effect of power systems	9
2.4	Load-frequency control mechanism.....	11
2.4.1	Primary control reserve (FCR)	12
2.4.2	Secondary control reserve (aFRR)	18
2.4.3	Tertiary control reserve (mFRR).....	18
2.5	Additional control schemes	19
2.5.1	Automatic low-frequency demand disconnection (LFDD)	19
2.5.2	Limited-frequency-sensitive-mode (LFSM)	20
3	Model.....	21
3.1	Modelling approach	22
3.1.1	Inertial response behavior.....	22
3.1.2	Self regulating effect.....	23
3.1.3	Primary control.....	23
3.2	Model discussion	24
4	Methodology	26
4.1	Data processing	27
4.1.1	Frequency measurements processing.....	28
4.1.2	System size determination	29
4.1.3	System inertia determination	31
4.2	RoCoF zero crossing method.....	34
4.2.1	RoCoF calculation.....	34
4.2.2	Detection of RoCoF zero	35
4.2.3	Mathematical formulation of the RoCoF zero crossing method.....	36
4.3	Fix supporting points method	40
4.4	Optimal fit method	42
4.4.1	Optimization approach.....	42

5	Results	44
5.1	RoCoF zero crossing method	44
5.2	Fix supporting points method	47
5.3	Optimal fit method	49
5.4	Comparison between the methods.....	54
5.5	Statistical analysis.....	55
6	Conclusion	58
	LIST OF FIGURES	60
	LIST OF TABLES	62
	LIST OF REFERENCES	63
	ANNEX	65
A	Graphical User Interface	65
B	Table of the results	66

1 Introduction

This chapter introduces the background and motivation of this thesis. Moreover, the research question is raised and the applied methods are presented. Finally, the structure of this thesis is discussed.

1.1 Background and motivation

Tackling the imminent climate crisis is one of the most important challenges of humankind today. Stabilizing the climate change requires strong, rapid, and sustained reductions in greenhouse gas emissions. To achieve a net zero carbon dioxide emission balance a fundamental shift to a sustainable energy supply chain is essential.

This requires a significant change on the supply and on the demand side in electrical power systems. Due to the transition to renewable energy sources, the penetration of power electronics interfaced generation (PEIG) rapidly increases [1]. Conventional generation plants using synchronous machines to feed into the grid are increasingly being substituted by PEIG-units, such as those using wind and solar. PEIG-units do not inherently provide inertia, thus a decrease of synchronous machines based generation leads to a reduction of power system inertia. This reduction makes power systems more prone to frequency instabilities [2].

In addition to the reduction of the power system inertia, a reduction of the self regulating effect of power systems (SRE) is forecasted [3]. This SRE is mainly based on uncontrolled loads, by changing their consumption as a function of the power system frequency. An increasing number of uncontrolled loads (e.g. asynchronous motors) are being replaced by drives with frequency converters. This results in a lower SRE. The size of the resulting frequency deviation in response to a power imbalance strongly depends on the SRE and the inertia of the power system.

An accurate SRE value with respect to the load mix and daily, weekly or seasonal patterns is important for an accurate modelling of the system frequency response to a power imbalance. A reliable frequency response model is crucial to determine the appropriate dimensioning of the Frequency Containment Reserve (FCR) and system defence plan measures needed for a secure power system operation.

1.2 Major objective of the thesis and applied method

The aim of this thesis is to identify the SRE based on dynamic power system characteristics using a top-down-approach. A top-down approach with three different methods is used to identify the SRE and the composition of the power system frequency characteristic (K-factor) based on real frequency events. This work questions the established planning values for the SRE of 1-2 %/Hz and investigates the necessity for adjustment. Furthermore, patterns or correlations of the effect with prevailing conditions (daily, weekly, seasonal dependency) are investigated to improve the predictability.

1.3 Structure of the thesis

This thesis is organized as follows. Chapter 2 gives a theoretical input for the further work. Chapter 3 presents the model used and the detailed underlying components. Subsequently, Chapter 4 shows the methodology by presenting all three methods used. The workflow from data processing to the extraction of the results will be also explained within this chapter. The results of the different methods are discussed in Chapter 5. Finally, Chapter 6 gives a conclusion and discusses possible sources of inaccuracies and recommendations.

2 Theory

According to [4] “power system stability can be defined as the stability of an electric power system, for a given initial operating condition, to regain a state of operating equilibrium after being subjected to a physical disturbance, with most system variables bounded so that practically the entire system remains intact.” Power systems are subjected to a wide range of disturbances, from small load changes to cascading events. Generally, power system stability is classified in three major pillars, depicted in Figure 1. During large disturbances all instability phenomena can appear simultaneously, or one form of instability may ultimately lead to another form [5]. Recently, Harmonic Stability related to the control structures of power electronics and FACTS devices has been added to the classification.

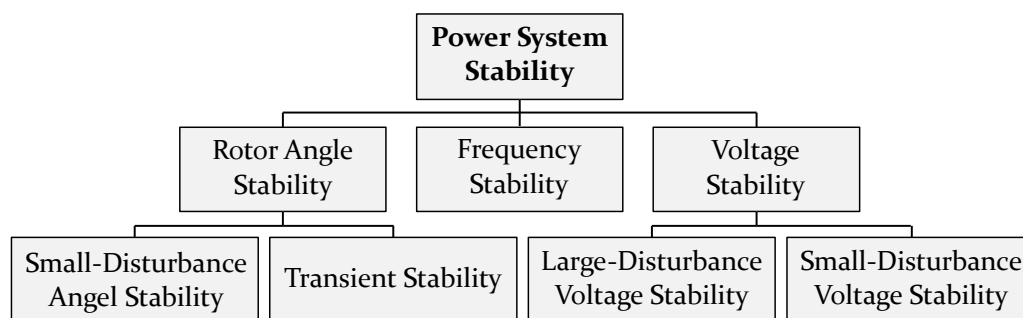


Figure 1: Classification of power system stability. Adapted from [5]

Frequency stability is an essential part of the overall stability of a power system. Therefore, the system frequency acts as an indicator for the quality and the stability of the grid. The system frequency is directly linked to the rotation speed of all grid connected synchronous machines. For a remaining stable frequency, the balance between supply and demand of electricity must be always given at all times. In other words, the active power needs to be generated at the same time as it is consumed, otherwise a frequency deviation occurs.

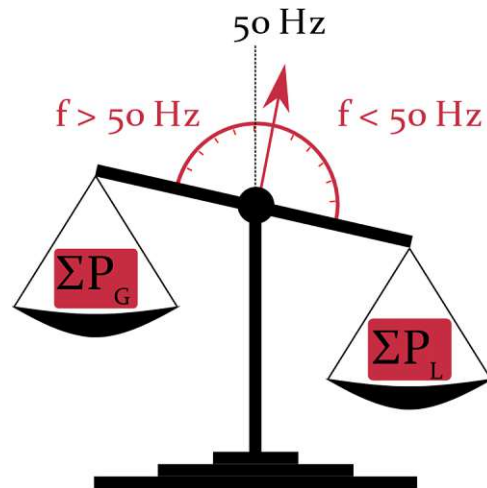


Figure 2: Balance between generation and load

As can be seen in Figure 2, if the load P_L exceeds the power supply by generation P_G , the system frequency will decrease and vice versa.

Due to a limited possibility to store electric energy, there is no sufficient way for controlling the power equilibrium in real-time only with storage units. Therefore, power systems need to have enough flexibility to react on either changes in demand or outages in generation and transmission [6]. Further details regarding the load-frequency control mechanism of a power system are described in chapter 2.4 .

2.1 Frequency response of synchronous machines

Synchronous machines are frequency determining factors in electrical networks. Consequently, understanding the behavior and the correlation of angular rotation speed to torques applied to the drive shaft is essential.

Based on the law of conservation of torques $\sum T = 0$ the differential equation of motion for a synchronous machine is described with the following equation:

$$J \cdot \frac{d^2\delta}{dt^2} - T_m + T_{el} + T_D = 0 \quad 2.1$$

with a closer look on

J : moment of inertia in $kg\ m^2$,

- $J \cdot \frac{d^2\delta}{dt^2}$: resulting torque is equal to moment of inertia times angular acceleration \propto ($\alpha = \frac{d^2\delta}{dt^2}$) in Nm ,
- T_m : mechanical torque of the prime mover in Nm ,
- T_{el} : electromagnetic braking torque resulting from stator currents counteracting with the drive torque in Nm ,
- T_D : damping torque due to damping windings and/or flowing eddy-current in iron parts in Nm .

The damping torque is neglected for the following fundamental considerations. The damping winding is only active in case of deviation of the angular speed (frequency) of a single machine with regard to the rest of the synchronous grid. In a conventional power plant, the prime mover and the generator are connected through the same drive shaft. Accordingly, the balance between mechanical torque T_m (prime mover) and the electromagnetic torque T_{el} (generator) is responsible for any kind of changes in the angular acceleration.

With the simplified differential equation of motion (2.2), the relation of the angular speed ω_m of the shaft and difference of the torques is found:

$$J \cdot \frac{d^2\delta(t)}{dt^2} = J \cdot \frac{d\omega_m(t)}{dt} = T_m(t) - T_{el}(t) \quad 2.2$$

A change in angular speed is caused when there is an imbalance between the two referenced torques. The rate of change is indirectly proportional to the moment of inertia J of the synchronous machine. In general, the larger the moment of inertia J , the smaller the resulting angular speed deviation will be. This means, that heavy and large synchronous machines, for e.g. as found in nuclear power plants, are less sensitive to short-term torque imbalances [7], [8].

The relation between angular speed of the shaft ω_m and angular frequency of the electromagnetic field ω in the synchronous machine is described with the help of the number of pole pairs p .

$$\omega = p \cdot \omega_m \quad 2.3$$

$$P = T \cdot \omega_m \quad 2.4$$

For an easier further handling, these two relations are applied on formula 2.2. :

$$\frac{J}{p} \cdot \frac{d\omega}{dt} = \frac{P_m}{\omega_m} - \frac{P_{el}}{\omega_m} \quad 2.5$$

After rearranging and defining ΔP , the power difference, we obtain:

$$p \cdot \Delta P = p \cdot (P_m - P_{el}) = J \cdot \omega_m \cdot \frac{d\omega}{dt} \quad 2.6$$

With the help of the definition of the starting time constant T_A , the moment of inertia J is substituted in the next step. T_A is the time required for the power unit to accelerate from zero to nominal speed at constant nominal mechanical Torque $T_{m,n}$ under no load conditions. The starting time constant is therefore calculated as follows:

$$\omega_{m,n} = \int_0^{T_A} \dot{\omega}_m(t) dt = \frac{T_{m,n}}{J} \cdot T_A \quad 2.7$$

$$T_A = \frac{J \cdot \omega_{m,n}}{T_{m,n}} = \frac{J \cdot \omega_{m,n}^2}{S_n} = \frac{J \cdot \omega_n^2}{S_n \cdot p^2} \quad 2.8$$

After rearranging the equation for J , it results:

$$J = \frac{T_A \cdot S_n \cdot p^2}{\omega_n^2} \quad 2.9$$

The equation 2.6 and equation 2.9 are used to introduce a relationship between active power balance and angular speed deviation:

$$p \cdot \Delta P = J \cdot \omega_m \cdot \frac{d\omega}{dt} = \frac{T_A \cdot S_n \cdot p^2}{\omega_n^2} \cdot \omega_m \cdot \frac{d\omega}{dt} \quad 2.10$$

$$\Delta P = \frac{T_A \cdot S_n \cdot p}{\omega_n^2} \cdot \omega_m \cdot \frac{d\omega}{dt} \quad 2.11$$

and also considering $\omega_m = \frac{\omega}{p}$ and $\omega = 2\pi f$.

$$\Delta P = \frac{T_A \cdot S_n}{\omega_n^2} \cdot \omega \cdot \frac{d\omega}{dt} = \frac{T_A \cdot S_n}{f_n^2} \cdot f \cdot \frac{df}{dt} \quad 2.12$$

By rearranging on the gradient $\frac{df}{dt}$ and neglecting the fraction of $\frac{f_n}{f}$, as for small frequency deviations $\frac{f_n}{f} \approx 1$, the equation results to

$$\frac{df}{dt} = \frac{\Delta P}{S_n} \cdot \frac{f_n}{T_A} \cdot \frac{f_n}{f} \approx \frac{\Delta P}{S_n} \cdot \frac{f_n}{T_A} \quad 2.13$$

In the further analysis the inertia constant H^1 is introduced as ratio of kinetic energy of the synchronous machine to the nominal power S_n .

$$H = \frac{E_{kin}}{S_n} = \frac{\frac{1}{2} \cdot J \cdot \omega_{m,n}^2}{S_n} = \frac{1}{2} \cdot T_A \quad 2.14$$

T_A is substituted in equation 2.13 with the obtained relation $T_A = 2 \cdot H$.

$$\frac{df}{dt} \approx \frac{\Delta P}{S_n} \cdot \frac{f_n}{2 \cdot H} \quad 2.15$$

2.2 Inertia constant of the network

In the previous section 2.1, the frequency response behavior of a single synchronous machine responding to a specific step in the power balance has been discussed. However, the interest of this thesis, is to understand the frequency behavior of an entire electrical grid. Therefore, the analogy of a single machine to an entire system, considering an idealized network with a group of N synchronous machines, is used.

For the inertia constant H of the entire grid, a concept of Centre of Inertia (COI) is used, defined as the inertia center H_{Sys} of all generators connected to the grid.

$$H_{Sys} = \frac{\sum_1^n H_{SG,n} \cdot P_{SG,n}}{P_{Sys}} \quad 2.16$$

The frequency deviation as a function of the power imbalance ΔP , the system size P_{Sys} and their system inertia constant H_{Sys} is the basis for further analysis.

$$\frac{df}{dt} \approx \frac{\Delta P}{P_{Sys}} \cdot \frac{f_n}{2 \cdot H_{Sys}} \quad 2.17$$

The power imbalance ΔP is defined as sum of all active power generated minus sum of all active power consumed including the system losses.

$$\Delta P = \sum_i P_{Gi} - \sum_j P_{Lj} \quad 2.18$$

¹ While T_A is the time required for the power unit to accelerate from zero to nominal speed at constant nominal mechanical torque under no load conditions, H is the time required for the power unit to accelerate from zero to nominal speed at constant nominal power under no load conditions.

Estimations of the total kinetic energy $E_{Sys} = H_{Sys} \cdot S_{Sys}$, which is closely linked to the system inertia H_{Sys} , can be seen in Figure 3. The graph shows the yearly course of total kinetic energy of the Continental European (CE) power grid.

As can be seen below, the total kinetic energy depends on the daily and seasonal generation mix, which corresponds to the demand pattern. In the winter months, the total kinetic energy is typically higher than in the summer months, which is due to higher loads.

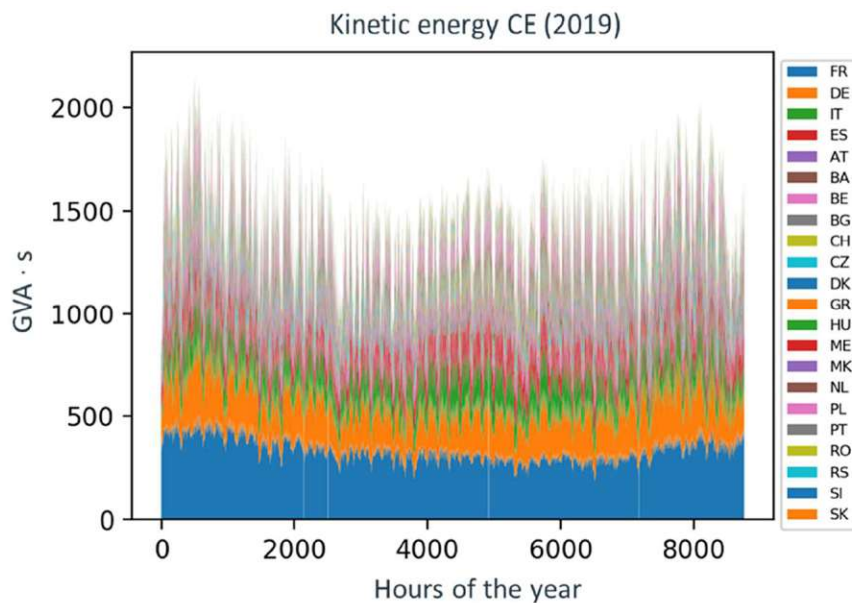


Figure 3: Kinetic energy of CE [7]

Figure 3 furthermore shows, that the main providers of kinetic energy are countries with the highest load in the CE power system. Particularly France (blue color) can be considered as a “solid backbone” of the systems kinetic energy, due to its high percentage of nuclear generation.

In case of a sudden power imbalance, a high kinetic energy of the system is important, because the power difference (deficit or surplus) is compensated in the first seconds only by the energy of the rotating masses of the synchronous machines. Synchronous machines provide this so-called inertial response, whereby their speed and thus their stored kinetic energy change accordingly. However, before the respective load-frequency control mechanism (chapter 2.4) interferes, the inertial response of rotating machines and the SRE(chapter 2.3) are damping the frequency deviation.

2.3 Self regulating effect of power systems

To understand the frequency behavior of an electrical grid it is necessary to discuss the frequency dependence of loads and power units connected to the grid. First of all, the SRE can be separated into two parts. On the one hand, the self regulating of power units and on the other hand the self regulating of loads can be found.

The self regulating effect of power plants is based on the speed control of municipal and industrial power plants [3].

The load self regulating effect describes an automatic and instantaneous adjustment of power consumption as a function of frequency. Like the inertial response of rotating machines, the load self regulating effect is an intrinsic mechanism, acting in real time, while damping damps the frequency deviation.

This is mainly based on the fact, that machines driven by asynchronous motors consume less power when the frequency, and thus the rotation speed, decrease. The other way around, an increase of frequency leads to an increase of rotation speed and therefore a higher power consumption.

In case of a stepwise frequency deviation, due to a power outage, the power consumption of all e.g. asynchronous motors also drop from power-speed characteristic A to characteristic B (1 to 2).

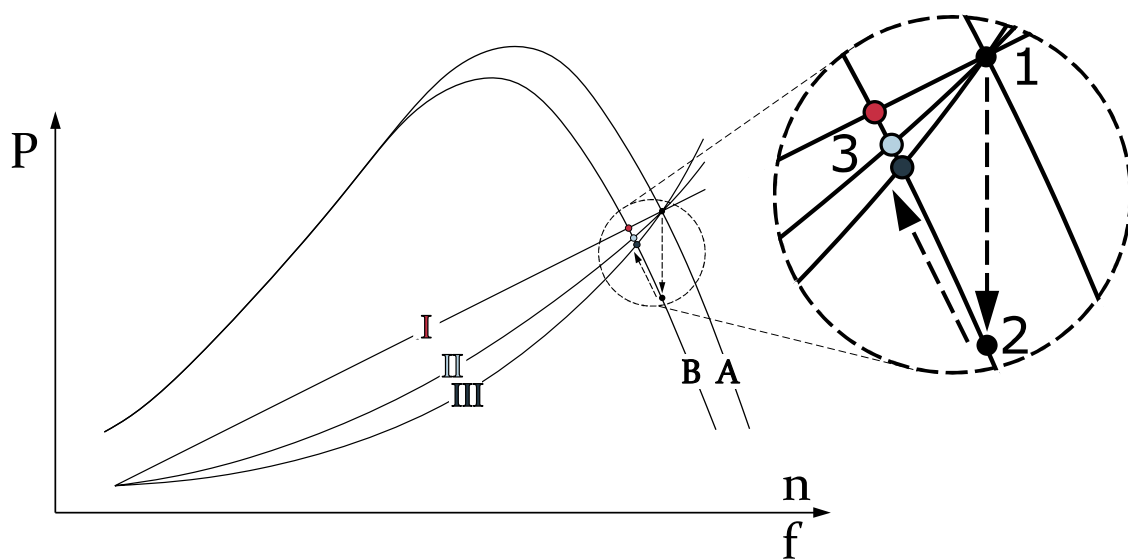
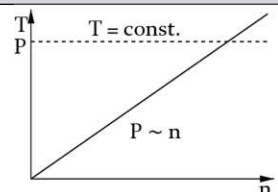
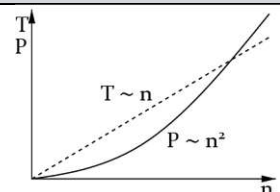
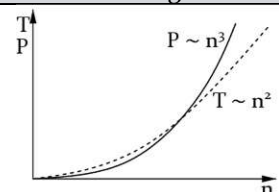
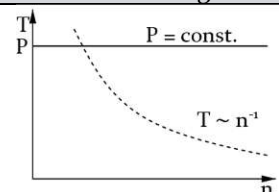


Figure 4: ASM and working machine behavior. Adapted from [3]

With withdrawing of the rotation energy within 1 second, a new steady-state operation point (3) is established along the new power-speed characteristic B. Depending on the speed-characteristics of the working machine the resulting operation point (intersection point of driving machine and working machine) has a different power consumption.

Working machines have different characteristics and can be classified into the following four groups with:

Table 1: Classes of load torques. Adapted from [9]

Torque constant	Torque linearly rising	Torque quadratically rising	Torque reciprocally decreasing
 <p>$T = \text{const.}$ $P \sim n$</p> <p>Conveyors, Cranes Extruders, Piston pumps, Compressors</p>	 <p>$T \sim n$ $P \sim n^2$</p> <p>Calenders</p>	 <p>$P \sim n^3$ $T \sim n^2$</p> <p>Turbomachinery, Centrifugal pumps, Cenrifuges, Blowers</p>	 <p>$P = \text{const.}$ $T \sim n^{-1}$</p> <p>Roller presses, Lathes</p>

The frequency-power behavior of individual loads or consumer collectives is different and can be described by a so-called consumer characteristic curve. Using a linearization of the consumer curve around the operation point, the parameter K_{Load} in MW/Hz for each load can be defined:

$$K_{Load} = \frac{\Delta P}{\Delta f} \quad 2.19$$

The parameter K_{Load} has a strong variation on the different load types and some exemplary k_{Load} -values, based on nominal power, are displayed in the following Table:

Table 2: k_{Load} per technology and examples. Adapted from [10]

Technology	k_{Load} in %/Hz	Example
	-2	Fluorescent lamps
Universal motor	-1	Refrigerator, winding machines
Resistive loads, controlled supply	0	Bulb, drive with frequency inverter
ASM with $T=\text{const}$	1-2	Conveyors, cranes, extruders
ASM with $T \sim n$	3-4	Calenders
ASM with $T \sim n^2$	5-6	Turbomachinery, centrifugal pumps

K_{SRE} represents the load power dependency on the frequency of all loads connected to the grid. With the analogy of a single machine in 2.18, K_{SRE} is defined as fraction between occurred power imbalance and resulting frequency drop.

After the power imbalance ΔP is brought to p.u. values with the system load P_{Sys} , the SRE k_{SRE} can now be described:

$$k_{SRE} = \frac{\Delta P / P_{Sys}}{\Delta f} \text{ in } \frac{\text{p.u.}}{\text{Hz}} \quad 2.20$$

The frequency response of loads of the entire grid can be expressed with the following formula:

$$P_{Load} = P_{Sys} \cdot (1 + k_{SRE} \cdot \Delta f) \quad 2.21$$

with $\Delta f = f - f_n$

As can be seen in equation 2.21, the power consumption of the load decreases when the frequency decreases and vice versa.

2.4 Load-frequency control mechanism

As already mentioned above, the inertial response of rotating machines and the SRE can damp, but not adequately stabilize an occurring frequency deviation. Therefore, to ensure only small deviations from the nominal frequency (50 Hz), a load-frequency control mechanism is crucial. This mechanism is responsible for compensating power imbalances, which leads to frequency deviations.

In the CE power system, the load-frequency control mechanism is structured into three levels of control reserves:

- Primary Control Reserve/ Frequency Containment Reserve (FCR)
- Secondary Control Reserve / Automatic Frequency Restoration Reserve (aFRR)
- Tertiary Control Reserve / Manual Frequency Restoration Reserve (mFRR)

The chronological activation of frequency control in the CE power system following a loss of generation is shown in Figure 5 and described in detail in the following subchapters.

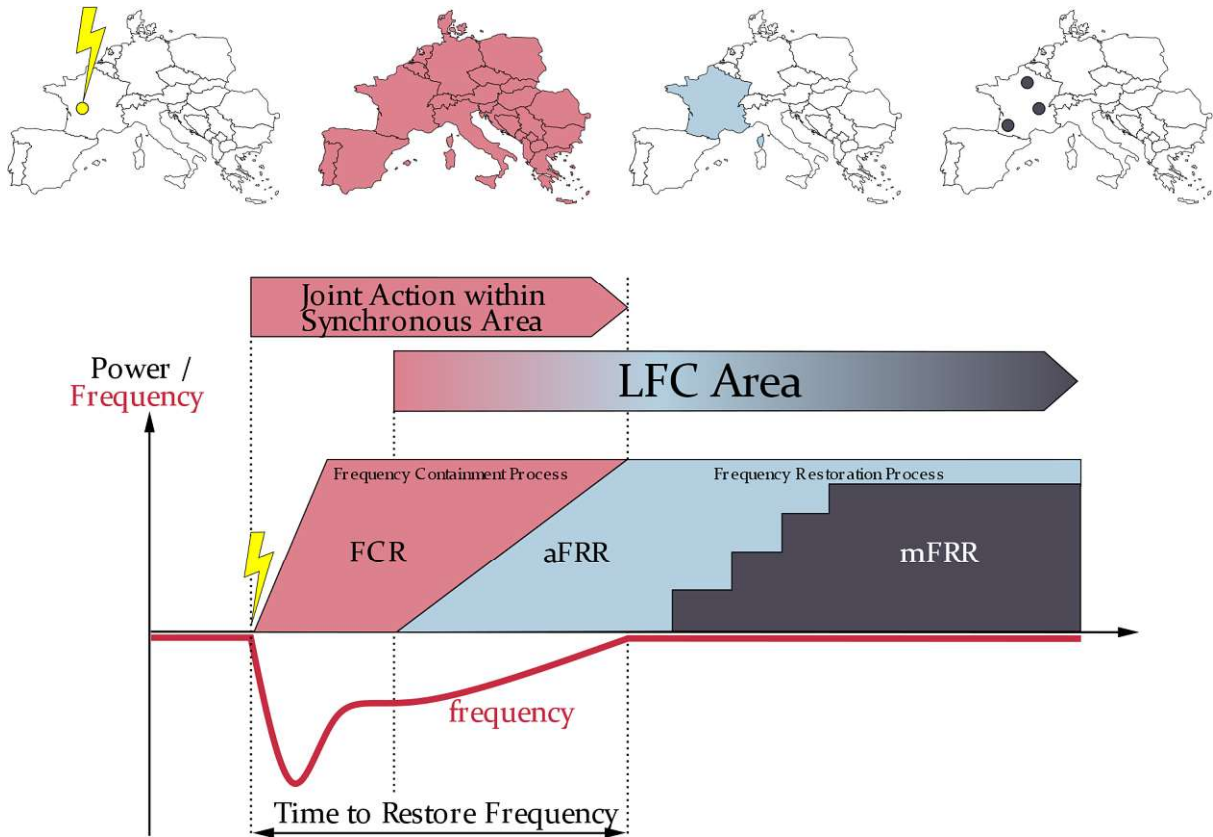


Figure 5: Activation of load-frequency control. Adapted from [11]

2.4.1 Primary control reserve (FCR)

The primary control reserve (FCR) and its underlying concept can be understood as a collective involvement of all control areas within a power system. It ensures that the frequency drop is intercepted and thus the grid frequency is stabilized at a quasi-steady-state value. Based on the operating point of the FCR providing units, active power activation is automatically triggered by the integrated controller and its droop characteristics as soon as a frequency deviation is detected (Figure 6). Generally, FCR-providing units must have the capability to increase or reduce their maximum allocated amount of FCR in each operating point (Figure 7). Until the system frequency is stabilized the controller of each FCR providing unit alters the active power based on the current frequency deviation. At the time the power balance is reestablished, the frequency remains at a quasi-steady-state value, but deviates from the nominal frequency, due to the droop of each FCR providing unit (P-controller) [6].

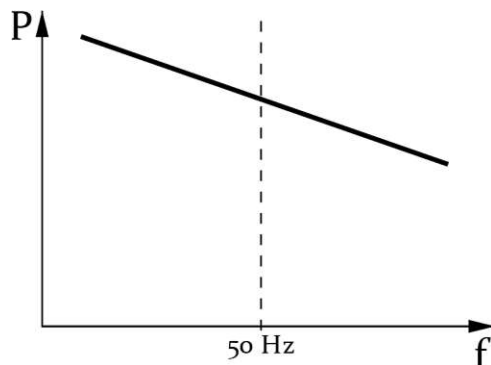


Figure 6: Primary control characteristic

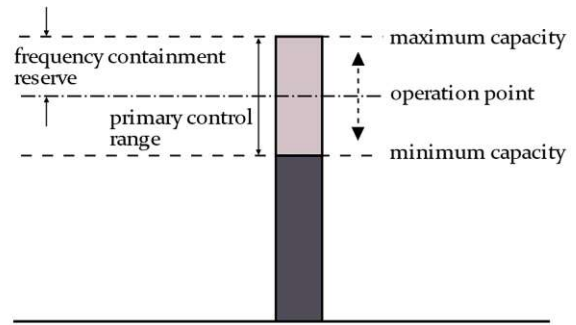


Figure 7: Operation point. Adapted from [12]

2.4.1.1 Minimum technical requirements for FCR in CE

The guideline on electricity transmission system operation (SOGL) from the European Commission, sets minimum technical requirements for FCR for each synchronous area within the European Union. As can be seen in Table 3, the minimum technical requirements differ depending on the synchronous area.

Table 3: FCR properties in different synchronous areas. Adapted from [13]

FCR full activation time	CE	30 s
	GB	10 s
	IE/NI	15 s
	Nordic	30 s
FCR full activation frequency deviation	CE	± 200 mHz
	GB	± 500 mHz
	IE/NI	± 500 mHz (dynamic FCR)
		± 1000 mHz (static FCR)
Nordic	± 500 mHz	

FCR providing units in the CE power system, shall additionally comply with the following Guideline requirements [13]:

- the activation of FCR shall not be artificially delayed and shall begin as soon as possible after a frequency deviation is detected;
- the maximum combined effect of inherent frequency response insensitivity and a possible intentional frequency response dead band of the FCR providing units shall not be greater than 10 mHz;
- at a frequency deviation equal to or larger than 200 mHz:
 - 50 % of the full FCR capacity shall be delivered at the latest after 15 seconds;

- 100 % of the full FCR capacity shall be delivered at the latest 30 seconds;
- Activation shall rise at least linearly from 15 to 30 seconds;
- At a frequency deviation smaller than 200 mHz, the activated FCR shall be at least proportional with the same time behavior referred above

These requirements leave room for interpretation of the different dynamics of FCR activation (Figure 8). The solid line shows a linear behavior up to the maximum FCR capacity, which equals the reference incident according to the SOGL. For imbalances smaller than the maximum FCR capacity, the dashed line characteristic would also meet the minimum requirements, but shows a significantly slower activation. The dynamic behavior represented by a PTI-element with an exemplary time constant τ of 6 s, exceeds the minimum requirements and comes closest to the real behavior of FCR-providing units (e.g. thermal power plants) in the CE power system.

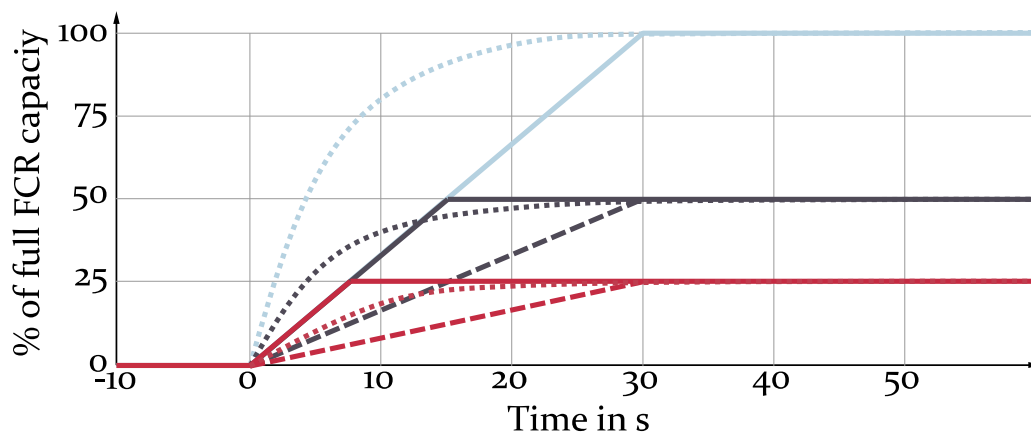


Figure 8: Dynamic options of FCR

2.4.1.2 Dimensioning of FCR / ENTSO-E Design Hypothesis

According to the SOGL the required FCR reserve capacity for the synchronous area shall cover at least the reference incident, which is equal to ± 3 GW in the CE power system. Based on the Design Hypothesis presented in annex AI of the former Union for the Co-ordination of Transmission of Electricity (UCTE) operational handbook [6], the FCR must be capable to compensate a sudden loss of 3 GW, without the need for automatic load shedding. The first stage of automatic load shedding occurs at 49 Hz. In addition, the quasi-steady-state frequency deviation after primary control shall not exceed 180 mHz, considering a SRE of 1 %/Hz. If no

SRE is considered, the quasi-stationary frequency deviation must not exceed 200 mHz. Figure 9 shows the simulated system frequency for the defined Design Hypothesis.

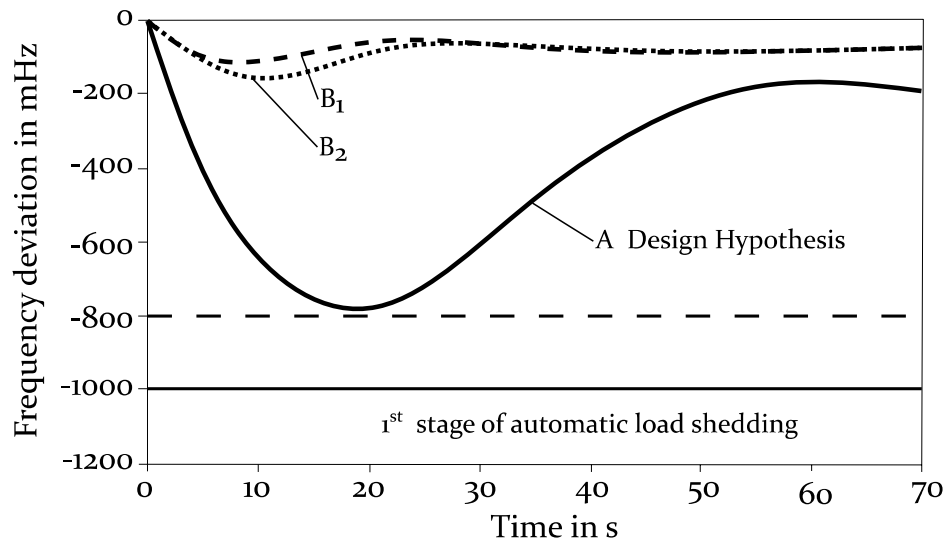


Figure 9: Design Hypothesis according UCTE. Adapted from [6]

The assumptions for the European Network of Transmission System Operators for Electricity (ENTSO-E) Design Hypothesis are listed below:

- Loss in generating capacity: $\Delta P = 3$ GW
- System load: $P_{\text{Sys}} = 150$ GW
- SRE: $k_{\text{SRE}} = 1$ %/Hz
- System start time constant: $T_A = 10 \dots 12$ s

This means that in the worst case (case A), a power imbalance of 3 GW under low load condition 150 GW occurring at nominal system frequency, leads to a maximum permissible dynamic frequency deviation of ± 800 mHz and a quasi-steady-state deviation of ± 180 mHz. For the maximum dynamic deviation there is still a safety margin of 200 mHz, before automatic load shedding will be activated. Theoretically, all power imbalances smaller than the reference incident must lead to a smaller frequency deviation than the Design Hypotheses (case B₁ and B₂).

2.4.1.3 Allocation of FCR in each control area

Each control area contributes to the FCR in proportion to its annual generation and load. The contribution coefficient is recalculated annually by ENTSO-E. For the year 2021, APG as control area operator needs to have ± 71 MW FCR permanently available [14].

2.4.1.4 Calculation of the K-factor

The shape of a frequency deviation can be described by the magnitude of the dynamic frequency deviation and the quasi-steady-state deviation (Figure 10). The dynamic frequency deviation (nominal frequency to frequency nadir) is mainly governed by the system start time constant T_A , SRE, system size and dynamics of the FCR providing units. The quasi-steady-state deviation is governed by the power system frequency characteristic – so-called K-factor. Since nominal frequency f_n is rarely given at the time of the incident, a new quantity, the change of quasi-steady-state deviation, is introduced.

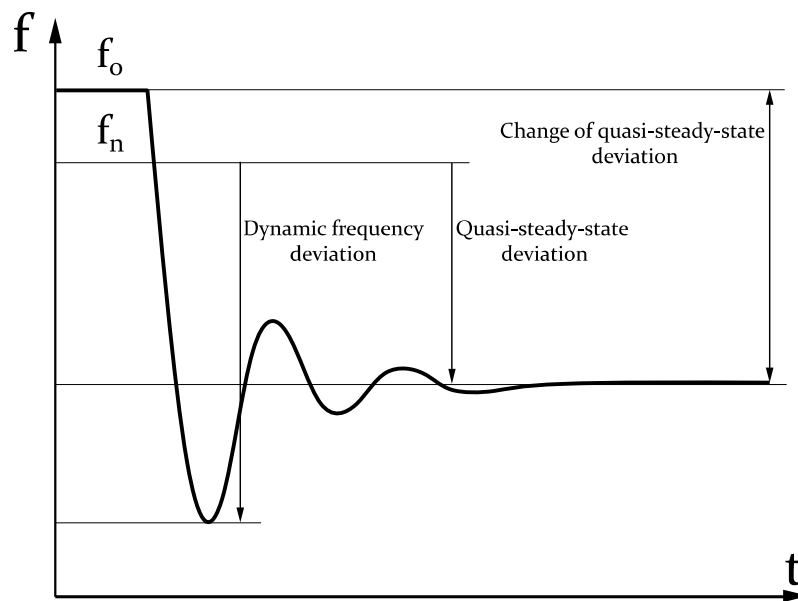


Figure 10: Dynamic and quasi-steady-state deviation. Adapted from [6]

The K-factor is mainly influenced by the total amount of FCR providing units and the SRE within the synchronous area.

This factor can be calculated as following:

$$K_{grid} = \frac{\Delta P}{\Delta f} \quad 2.22$$

with

ΔP : variation of power causing a disturbance,

Δf : change of quasi-steady-state frequency deviation in response to a disturbance.

Since real frequency responses do not show a smooth curve as in Figure 10, it might be difficult to determine the change of quasi-steady-state deviation Δf . For this purpose, an average

frequency methodology is used according the established ENTSO-E K-factor calculation. For the calculation, a linear regression is applied for an interval before and after the incident. The regression curve of the first interval, 10 seconds before the incidents until the time of the incident, is calculated and the value on the regression curve at -5 seconds (f_{-5}) is extracted. For the second interval, between 10 seconds and 30 seconds after the incident, the regression curve value at 20 seconds (f_{20}) is used.

The change of quasi-steady-state deviation Δf can be described as a difference of the above discussed values:

$$\Delta f = f_{-5} - f_{20} \quad 2.23$$

The Figure II shows the calculation of the change of quasi-steady-state deviation Δf , where a linear regression is performed in the required intervals and the regression values are taken 5 seconds before and 20 seconds after the incidents.

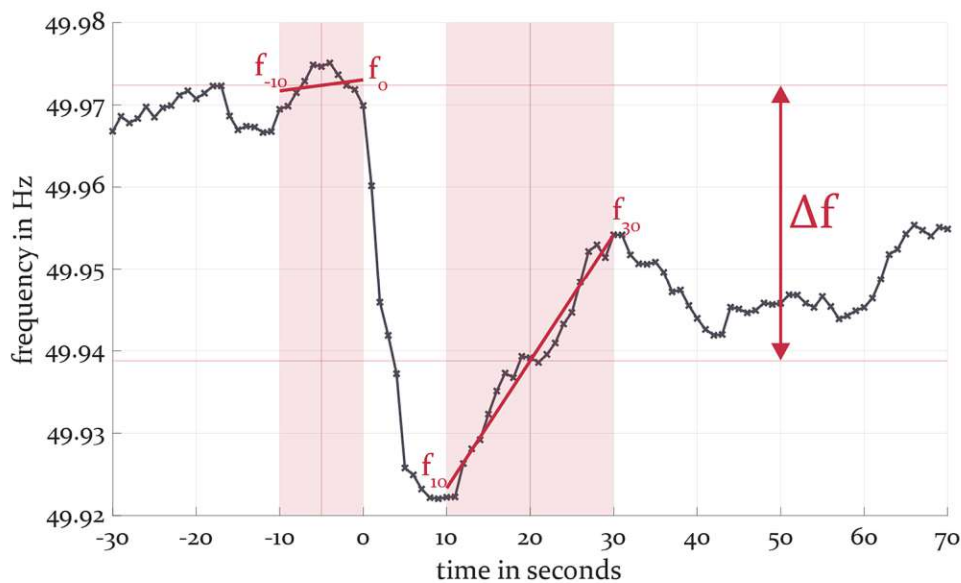


Figure II: Methodology for K-factor calculation

The K-factor is not a generally valid value or constant for all times and system states. It depends on the grid situation and is therefore calculated separately for each incident. An average K-factor can be calculated over all past disturbances.

2.4.2 Secondary control reserve (aFRR)

The task of secondary control is to maintain or to restore the power balance of each control area and thus to return the system frequency to its set-point value of 50 Hz. A respective power imbalance within a control area and the following joint action of primary control leads inevitably to a deviation of power interchanges with adjacent control areas to their programmed scheduled values. Only the secondary controller of the control area where the imbalance occurred is obliged to perform secondary control action. In order to avoid compensating the primary control activation in a control area, a Network Characteristic Method needs to be applied. According to this method, each control area needs to minimize the area control error (ACE) in real-time [6]:

$$ACE = P_{T,meas} - P_{T,prog} + K_{ri} \cdot \Delta f \quad 2.24$$

with

$P_{T,meas}$: measured active power transfers on the cross-border lines,

$P_{T,prog}$: programmed active power exchange program,

K_{ri} : K-factor of the control area in MW/Hz set on the secondary controller,

$\Delta f = (f - f_n)$: measured frequency deviation from nominal frequency set point.

In practice, the K_{ri} can be chosen slightly higher than the rated power system frequency characteristic, because the SRE is uncertain. If the controller detects an imbalance in its control area, a positioning command is automatically sent to the contracted aFRR providing units and needs to be executed within 5 min [6].

2.4.3 Tertiary control reserve (mFRR)

The function of the tertiary control reserve is to restore the range of the secondary control, in case a relevant power imbalance in the control area maintains for a significant time period (e.g. longer than 15 minutes). If the aFRR is not sufficient to cover the imbalance, additional mFRR can be activated within 15 minutes. This is done by manually requesting active power changes of the contracted mFRR providing units [4].

2.5 Additional control schemes

The three control reserves mentioned above can almost always keep the steady state system frequency deviation within a tolerable range of ± 200 mHz. For major incidents with larger resulting frequency deviations, additional mechanisms are defined and implemented in the national system defense plans according to the network code on electricity emergency and restoration (NC ER) from the European commission. The Austrian system defense plan, for instance includes the following mechanisms, as part of the frequency-plan [15]:

- Automatic low-frequency demand disconnection (LFDD)
- Limited-frequency-sensitive-mode (LFSM)

These additional control schemes should prevent critical network conditions and avoid major disturbances or limit their effects.

2.5.1 Automatic low-frequency demand disconnection (LFDD)

If the frequency drops more than 1 Hz, a stepwise automatic load shedding (LFDD) is activated. Figure 12 shows the implemented LFDD scheme according to the Austrian system defense plan. This LFDD scheme foresees at least six individual stages between 49,0 Hz and 48,0 Hz. As can be seen an automatic load shedding equal to 7 % of the system load must be realized at the first stage (49,0 Hz). Furthermore, a stepwise load shedding equal to 45 % of the system load has to be realized if the frequency reaches the last stage (48,0 Hz) [15].

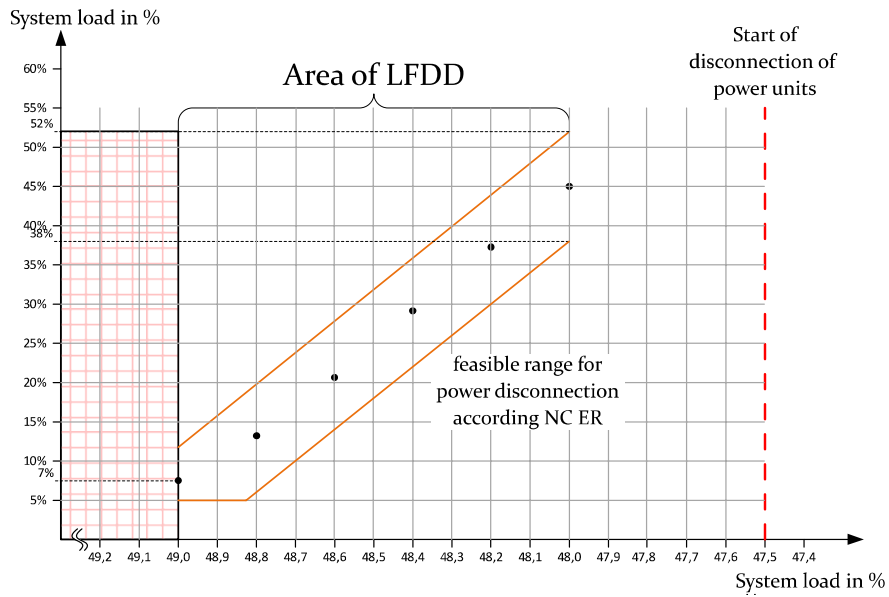


Figure 12: Sample for the Austrian LFDD-plan [15]

2.5.2 Limited-frequency-sensitive-mode (LFSM)

The Limited Frequency Sensitive Mode defines either an active power reduction in case of overfrequency (LFSM-O) or an active power increase in case of underfrequency (LFSM-U). As required in the Austrian national grid code (TOR) each generator type (Type A-D) must be capable to reduce its active power in case of overfrequency greater than 50,2 Hz with a default droop of 5 %. Larger generators (Typ C and D) must also be capable to increase their active power in case of underfrequency less than 49,8 Hz with a default droop of 5 % [16].

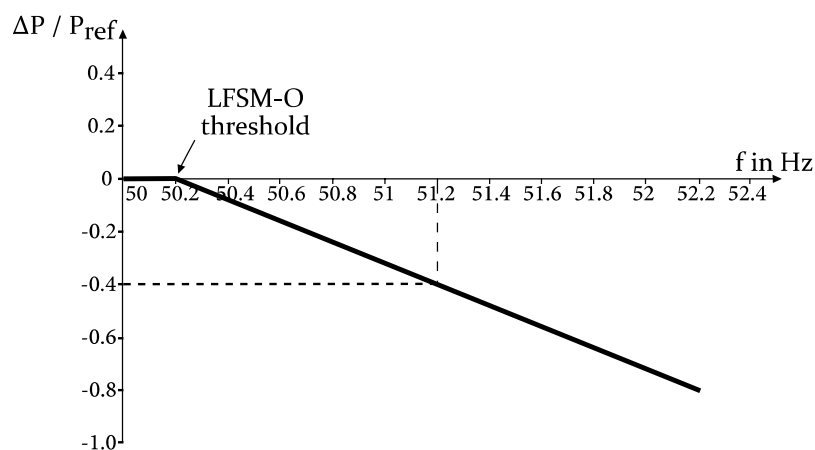


Figure 13: Scheme of LFSM-O behavior [16]

3 Model

The model is used to describe the frequency response of the CE power system. The simplified model, based on the principle of a harmonic oscillator, consists of two intrinsic mechanisms and one control reaction. The simplified model can be used only to describe the frequency response of the system in the time period between the occurrence of the imbalance and the full activation of the FCR (30 seconds) and no secondary control regime actions. By reducing the model complexity also unknown and superposed effects are reduced. The SRE is an instantaneous intrinsic mechanism and the importance decrease over time due to activation of the frequency control regimes.

Figure 14 shows the block diagram of the major model elements.

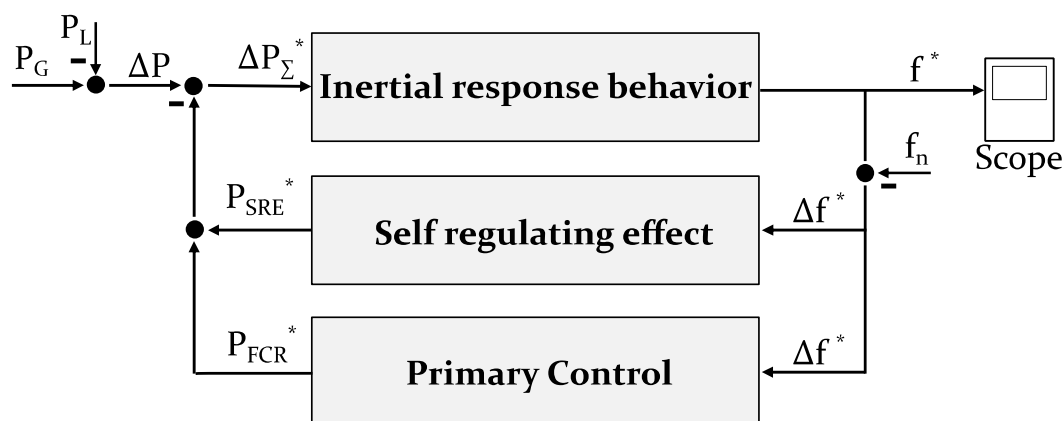


Figure 14: Block diagram of the balancing model

The model input is formed as the difference between the generated power P_G of the entire CE power system and the corresponding system load P_L . This power difference ΔP is almost zero in normal system operation. However, if a disturbance occurs, this power difference leads to a frequency deviation due to the changed rotation speed of the synchronous machines, as

described in chapter 2.1 . The time-dependent frequency behavior taking into account the stabilizing effects is the output of the model.

The block inertial response represents the behavior of all synchronous machines reacting to a power imbalance. A sudden power imbalance is compensated in the first seconds only by the energy of the rotating masses of the synchronous machines. Thereby, their speed and thus their stored kinetic energy change accordingly.

The SRE, like the inertial response, is an intrinsic mechanism and therefore reacts instantaneously to counteract the frequency deviation.

The primary control, as the first stage of the control reactions, intercepts the frequency drop and stabilizes the power system frequency on a quasi-steady-state value.

All intermediate results with an asterisk “*” are recalculated in each simulation step and are therefore time-dependent.

3.1 Modelling approach

Based on the reduced model shown in Figure 14 the block diagram is implemented with the Software MATLAB/Simulink. Following chapters will describe the block diagram in more detail.

3.1.1 Inertial response behavior

The inertial response behavior - all synchronous machines reacting to a power imbalance- can be modeled in a form of an integrator element. The inertial response behavior block describes the relation between power difference ΔP_{Σ}^* and frequency response f^* . The frequency gradient $\frac{df}{dt}$ is calculated using equation 2.17 and is integrated with the initial frequency f_0 .

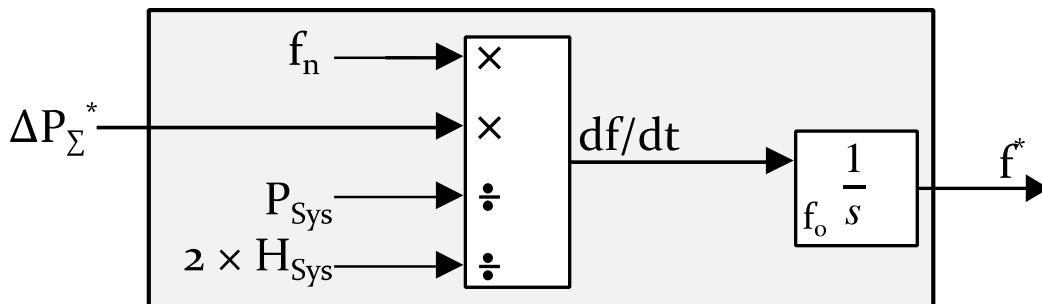


Figure 15: Block diagram of Inertial response behavior

3.1.2 Self regulating effect

The active power provided by the SRE is shown in Figure 16. Since only the balance between power generation and load is important for the system frequency, it makes no difference whether the SRE is treated as a reduction in load or, alternatively, as an increase in generated power. To calculate the active power P_{SRE}^* from the SRE, the frequency deviation ($\Delta f^* = f^* - f_n$) is multiplied by the SRE k_{SRE} times the system load P_{Sys} .

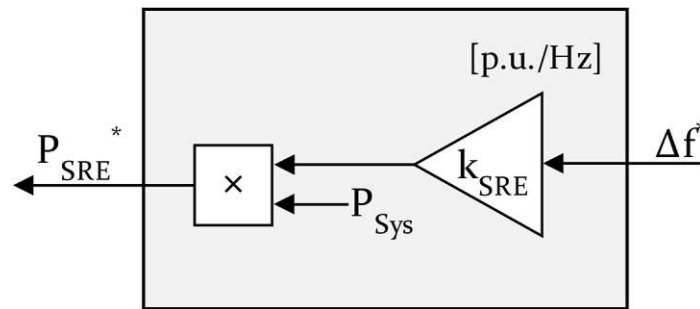


Figure 16: Block diagram of SRE

3.1.3 Primary control

The activation of the FCR is subject to the minimal requirements mentioned in chapter 2.4.1.1. Taking these requirements into account, the detected frequency deviation Δf^* is multiplied by the parameter K_{FCR} , which is equal to 3 GW/0.2 Hz = 15 GW/Hz. The saturation element limits the active power P_{FCR}^* to the maximum FCR ± 3 GW. Finally, a 6 seconds time constant T_1 for the PT1 transfer function is chosen to model the FCR ramp-up behavior. For simplicity, the maximum combined effect of inherent frequency response insensitivity and possible intentional frequency response dead band of the FCR providing units is not further taken into account.

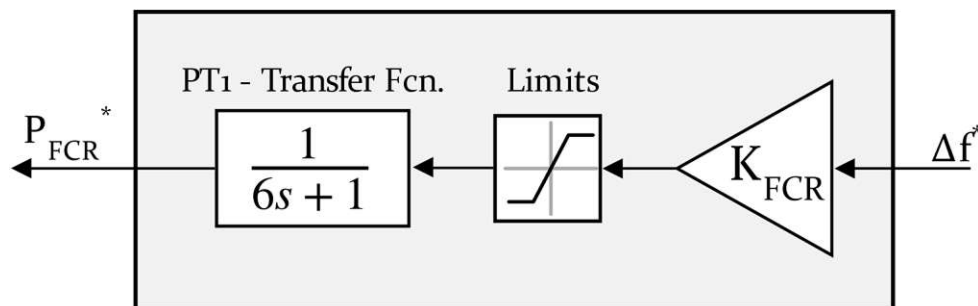


Figure 17: Block Diagram for primary control

3.2 Model discussion

The model, described in the sections above, is used to calculate and discuss the frequency response in case of a power imbalance. This model includes the corresponding behavior of the inertial response, the SRE and the FCR. For the example shown in Figure 18, the same assumptions are made according to the Design Hypotheses, defined in chapter 2.4.1.2.

As can be seen in Figure 18, the sum of inertial response, FCR and SRE always results in the actual power imbalance (dashed line). In the first seconds after a power imbalance the inertial response and SRE react instantaneously. With increasing frequency deviation, the contribution of SRE increases proportional and reaches its maximum at the frequency nadir. The slightly delayed FCR shows a typical PTI behavior and reaches its maximum after 30 s.

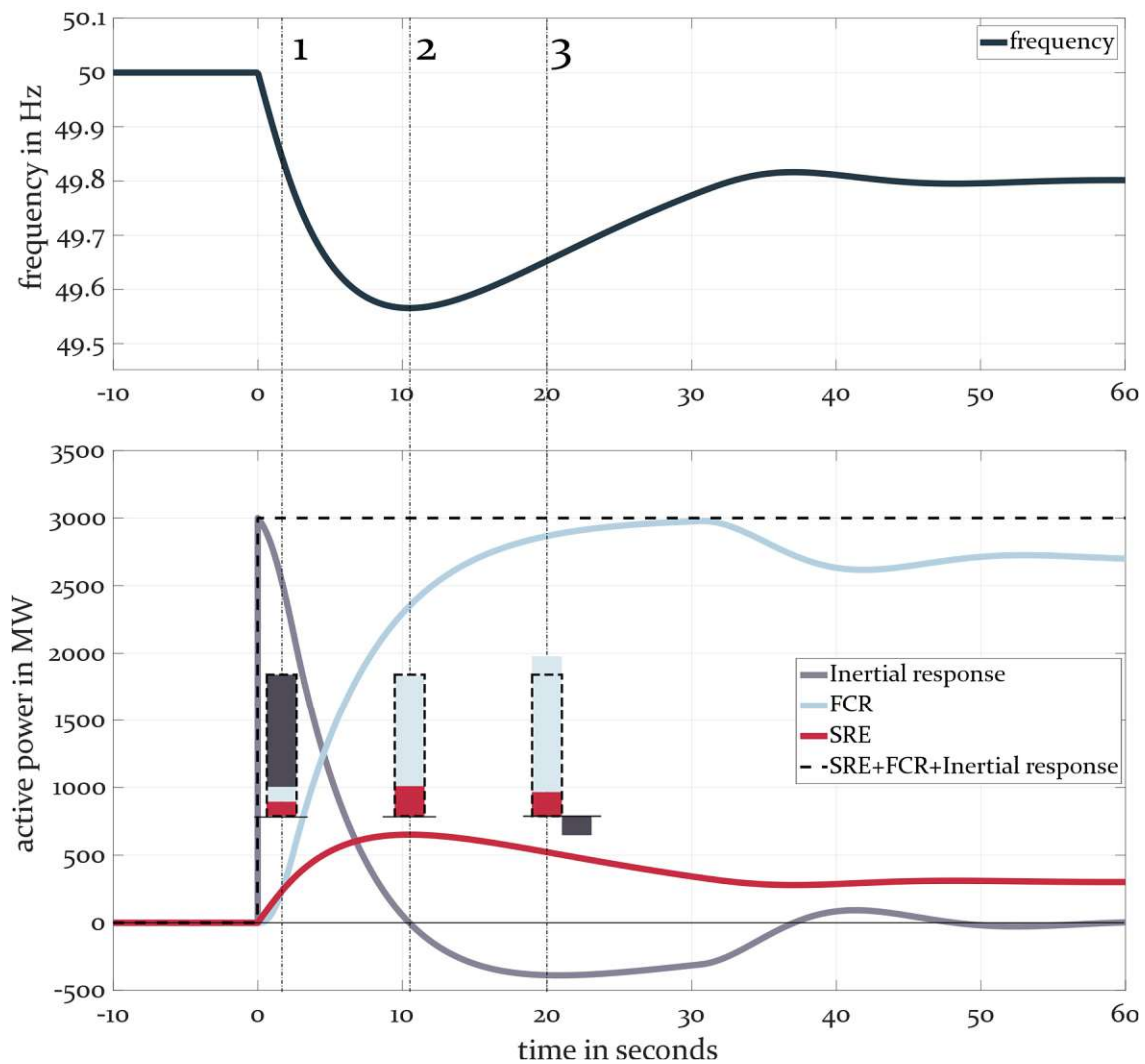


Figure 18: FCR, SRE-reaction to a power imbalance with resulting frequency deviation

The initially dominating inertial response (1) decreases rapidly and becomes zero at the time of the frequency nadir (2). As soon as the frequency drop is intercepted by the help of FCR and SRE, the inertial response becomes negative (3), since the gradient $\frac{df}{dt}$ becomes positive.

4 Methodology

The aim of this chapter is to describe the methodology used to determine the SRE based on historic dynamic power system states.

An overview of the methodology approach is shown in Figure 19. As a first step, data from frequency events larger than 1 GW are collected. These data sets are prepared and processed for the further analysis. Subsequently, three different methods are used to identify the composition of the K-factor for each individual event. Finally, a statistical analysis of the K-factor components (SRE and FCR) is performed. Within the statistical analysis the results are additionally analyzed regarding observable correlations and patterns.

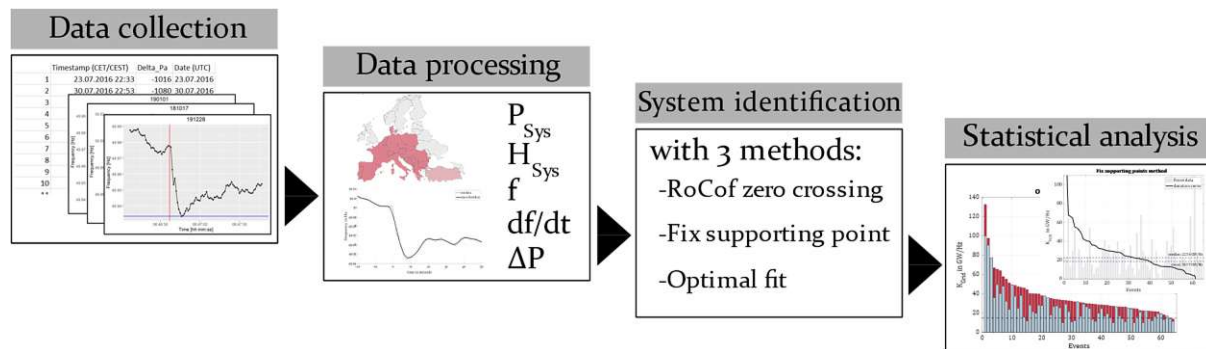


Figure 19: Overview of the methodology approach

Figure 20 shows the model used for the selected top-down system identification approach. Based on the available data from the collected events the yellow highlighted parameters are known or can be processed. The red and blue marked blocks represent the unknown parameters, namely the SRE k_{SRE} and the power system frequency characteristic of the FCR K_{FCR} . The following section 0 explains the preparation of the required input and output

parameters for the model and the three system identification methods to identify the unknown parameters.

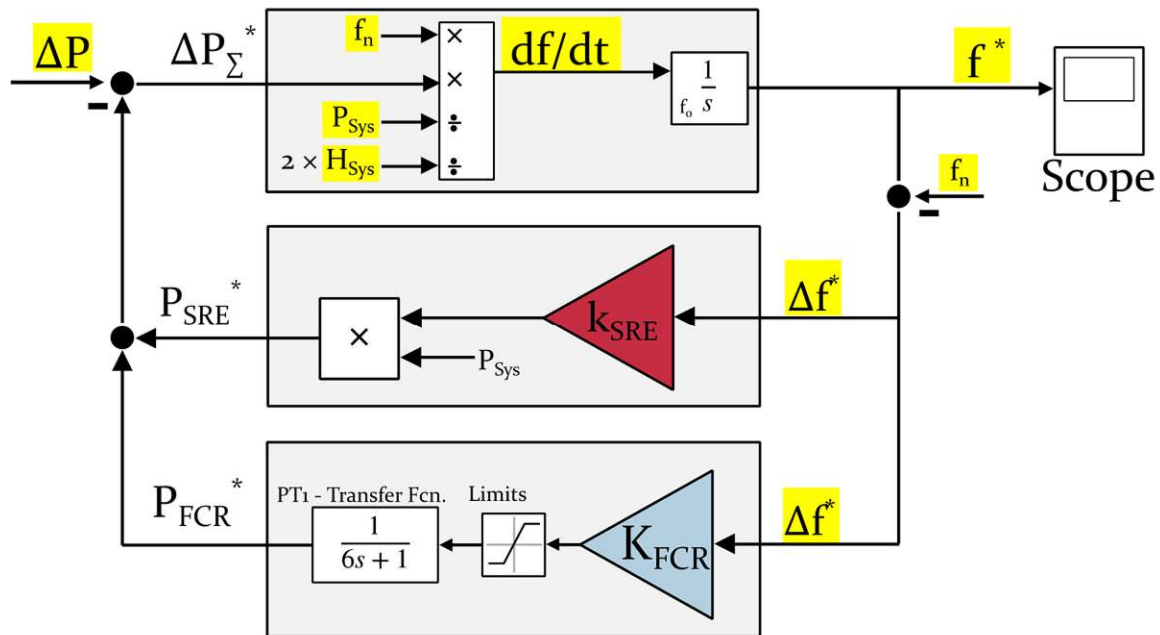


Figure 20: Simulation model with known (yellow) and unknown (red, blue) parameters

4.1 Data processing

For the study a minimum set of parameters needs to be known:

- ΔP : size of imbalance (power plant outage/ HVDC head-end station failure)
- f : measured frequency
- P_{Sys} : power system size/ total system load
- H_{Sys} : system inertia

As a basis for further investigations, data sets of 64 observed frequency events from 2016 to mid-2021 with imbalances larger than 1 GW were provided by the Austrian Transmission System Operator APG. A detailed overview of all events is given in Annex B.

The annual distribution of the events can be found in Table 4.

Table 4: Event distribution by year

Year	Events with (imbalance > 1 GW)
2016	10
2017	18
2018	12
2019	13
2020	9
2021	2
Σ	64

To get a better understanding of the selected data set, the daily and weekly distribution was analyzed. As can be seen in Figure 21, the distribution of the events appears to be inhomogeneous.

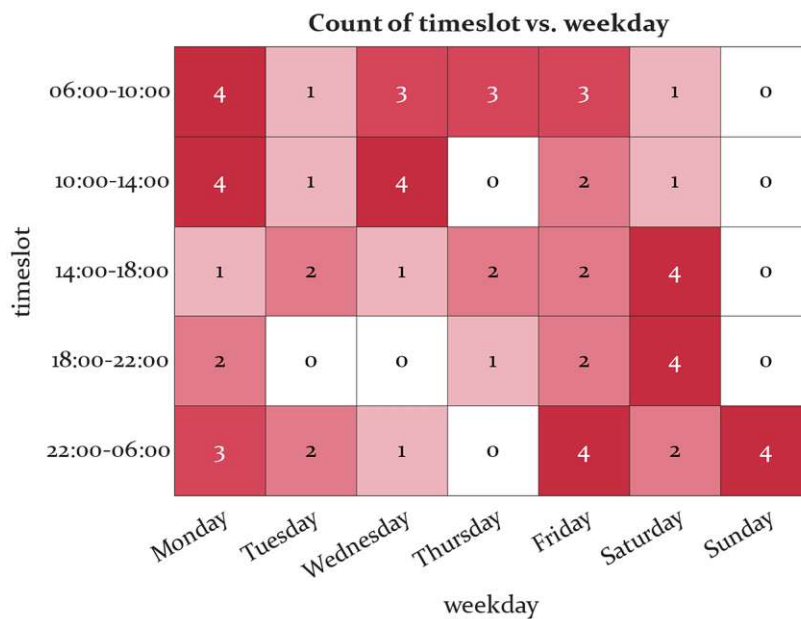


Figure 21: Events per timeslot per day

4.1.1 Frequency measurements processing

For this study, the frequency measurements of an APG substation (Wien Süd-Ost) were provided for each event. Given the raw frequency measurements an accurate estimation of the

start time of the imbalance event has to be made. With this information the frequency time series is truncated to 30 seconds before and 70 seconds after the event.

Figure 22 shows an exemplary processed time series. The small black squares indicate the measured values, the vertical red line represents the start time of the imbalance event and the blue horizontal line shows the frequency nadir.

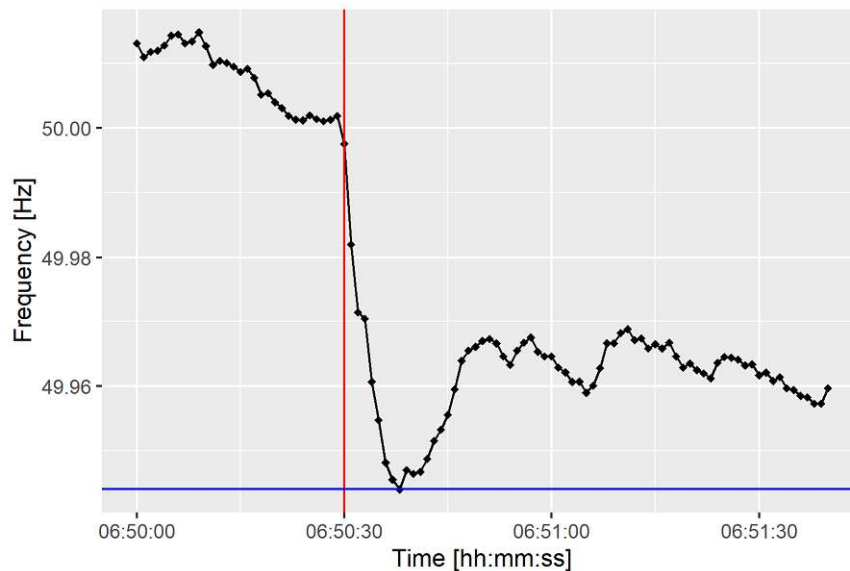


Figure 22: frequency measurements at 21.08.2017 – 06:50

4.1.2 System size determination

The Continental European power system is a synchronously connected area that consists of the following countries: Albania, Austria, Bosnia Herzegovina, Belgium, Bulgaria, Switzerland, Czechia, Germany, Denmark, Spain, France, Greece, Croatia, Hungary, Italy, Montenegro, North-Macedonia, The Netherlands, Poland, Portugal, Romania, Serbia, Slovenia, Slovakia and Turkey. All mentioned countries are official members of the ENTSO-E, except for Turkey. Turkey is declared as an observer member of the ENTSO-E. Figure 23 shows the so-called Regional Group Continental Europe (RGCE) marked in red.



Figure 23: Map of Regional Group Continental Europe

The ENTSO-E Transparency Platform [17] provides hourly load values per Control Area for all RGCE members except Turkey. To reconstruct the actual system load P_{Sys} of RGCE, the per unit load profile of the CE countries available on the Transparency Platform (CE TP) is calculated and scaled with the maximum load occurred in Turkey $P_{Turkey,max}$.

$$P_{Sys}(t) = \left(1 + \frac{P_{Turkey,max}}{P_{CE TP,max}}\right) \cdot \sum_{i=1}^{CE TP} P_i(t) \quad 4.1$$

At the time of research, a maximum load of 51 GW occurred in Turkey on the 02.07.2021 [18]. The adapted summed-up load profile of all RGCE countries can be seen below in Figure 24.

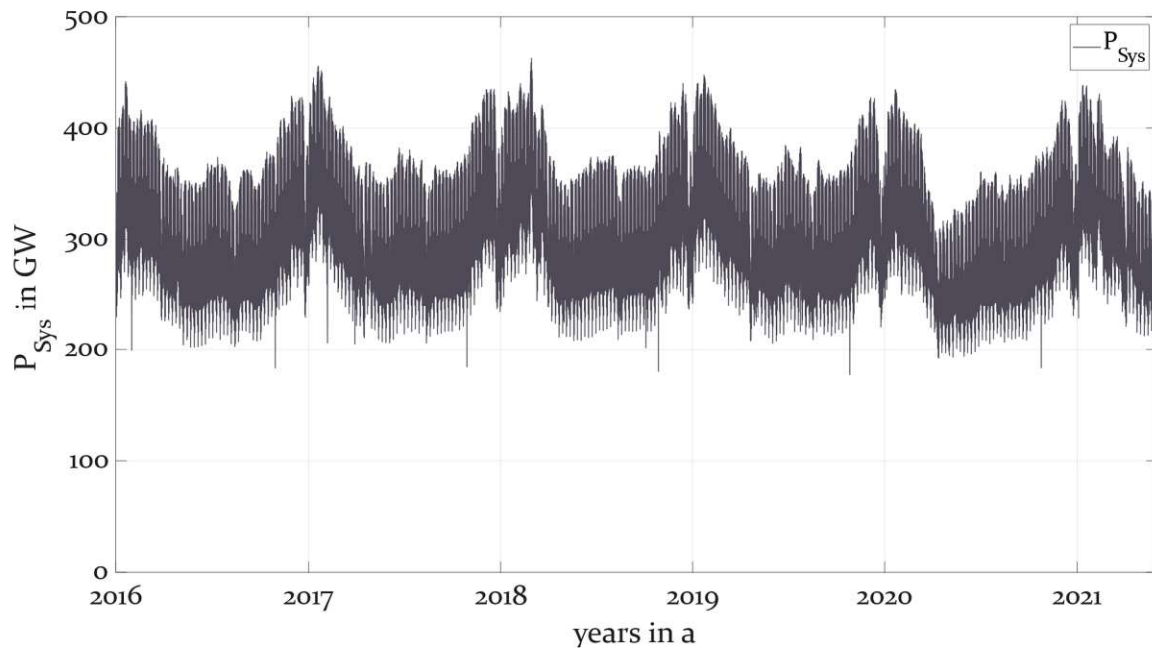


Figure 24: Calculated CE system load profile from 2016 to mid 2021

4.1.3 System inertia determination

In this chapter, the calculation of the system inertia constant H_{Sys} is explained. A concept of Centre of Inertia (COI) is used, which is defined as the inertia center of all generators connected to the grid. To estimate the H_{Sys} in the COI, a weighting factor w and a loading factor LF needs to be considered.

The weighting factor w considers the hourly generation mix per production type of the feeding power plant (data available on ENTSO-E Transparency Platform [17]).

$$w_i = \frac{P_{Type}}{P_{Total}} \quad 4.2$$

The loading factor (LF) describes the distribution of the generated power among several generation units. A LF of 1 means that the generating units are always operating at full capacity, and a LF of for example 0.5 describes an average of 50 % partial generation condition.

This information about the inertia and LF per production type is shown in Table 5:

Table 5: Inertia constant and loading factors per production type. Adapted from [7]

Production Type	Inertia H in s	Loading factor in p.u.
Nuclear	5.9	0.96
Fossil Oil	4.3	0.40
Fossil Hard coal	4.2	0.70
Fossil Gas	4.2	0.60
Fossil Coal-derived gas	4.2	0.54
Fossil Brown coal/Lignite	3.8	0.81
Fossil Peat	3.8	0.59
Other	3.8	0.56
Marine	3.8	0.50
Waste	3.8	0.28
Hydro Water Reservoir	3.7	0.56
Geothermal	3.5	0.83
Other renewable	3.5	0.50
Hydro Pumped Storage	3.5	0.46
Biomass	3.3	0.70
Hydro Run-of-river and poundage	2.7	0.61
Solar	0	-
Wind Offshore	0	-
Wind Onshore	0	-

Large generating units, such as nuclear power plants, provide large inertia constants, while inverter-coupled units, such as PV or most wind power plants, provide no inertia. For simplicity, the inertia of the rotating loads is neglected.

The total system inertia H_{Sys} is calculated considering the weighting factor and the loading factors for each production type i with the following equation.

$$H_{Sys} = \sum_i \frac{H_i \cdot w_i}{LF_i} \quad 4.3$$

The total system inertia H_{Sys} is calculated according to Equation 4.3 above. Figure 25 shows the results for the whole period of events.

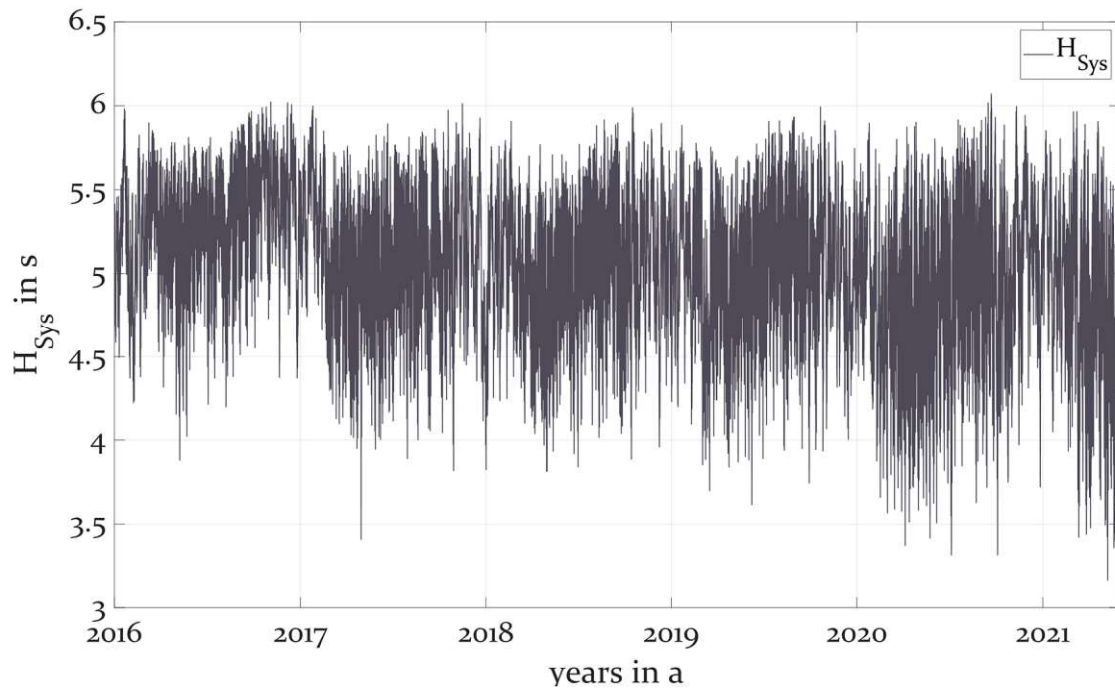


Figure 25: Calculated inertia profile from 2016 to mid 2021

4.2 RoCoF zero crossing method

This method is based on a system identification approach which uses the reduction of the model complexity in specific points in time. As shown in Figure 18, at the time of the frequency nadir, the Rate of Change of Frequency (RoCoF) is zero, that means no inertial response ΔP^* is taking place. If the RoCoF is zero, the occurred power imbalance ΔP is compensated only by the response of the SRE (P_{SRE}^*) and the activation of the FCR (P_{FCR}^*). The K-factor of FCR (K_{FCR}) and the SRE-Factor (k_{SRE}) are chosen in a way that their power response at the time of RoCoF zero (e.g. t_1, t_2) exactly corresponds to the imbalance ΔP . These points in time can be seen in Figure 26.

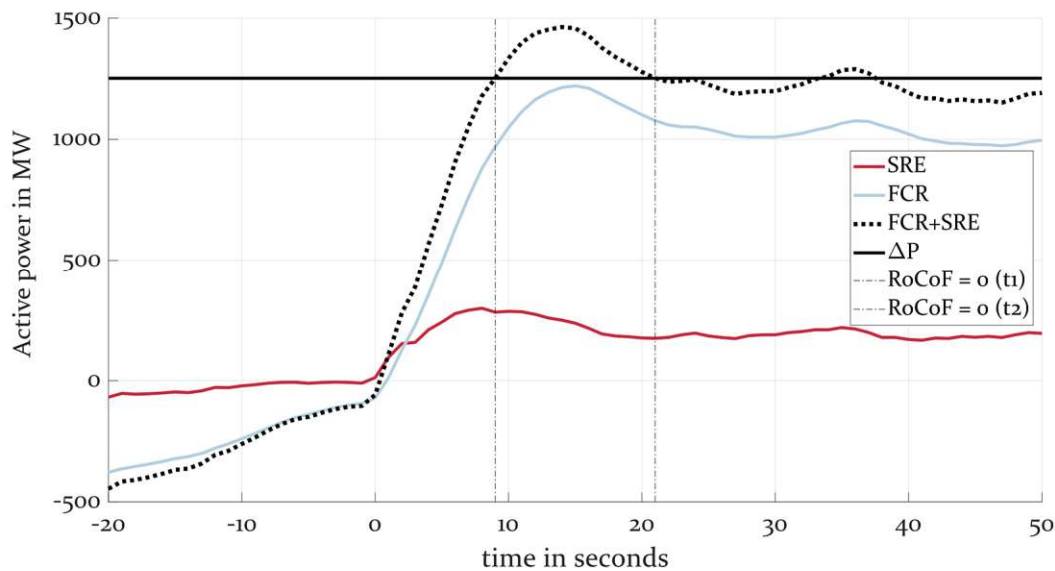


Figure 26: RoCoF zero crossing method for 21.08.2017-event

The procedure of this method is to determine the RoCoF, find its zero-crossings and choose the factors (K_{FCR}, k_{SRE}) for the condition mentioned above.

4.2.1 RoCoF calculation

Since real frequency responses do not show a smooth curve, the RoCoF calculation cannot be performed with a simple computation of the first derivative. Due to the noisy measurements, a smooth function is applied. The function smooths the frequency values within a 5 seconds window. An example of the smoothed frequency response can be seen in Figure 27 below.

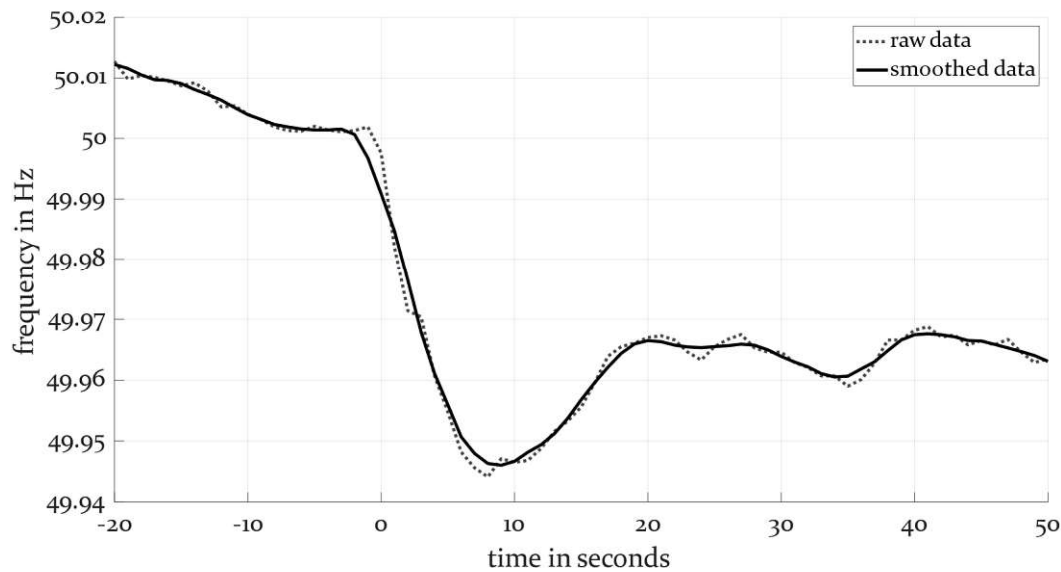


Figure 27: Smooth function applied on raw data

With the smoothed frequency response, a determination of the Rate of Change of Frequency (RoCoF) is done.

4.2.2 Detection of RoCoF zero

Considering real frequency measurements, it is unlikely to obtain RoCoF values, which are exactly zero. The RoCoF will be several times close to zero, but not exactly zero. Therefore, a directional detection is used with an additional condition that the smaller value in one second resolution around the exact estimated zero crossing is considered. This approach can be seen in Figure 28, the RoCoF-zero-crossing is detected (vertical lines), when the RoCoF changes from positive to negative values or vice versa.

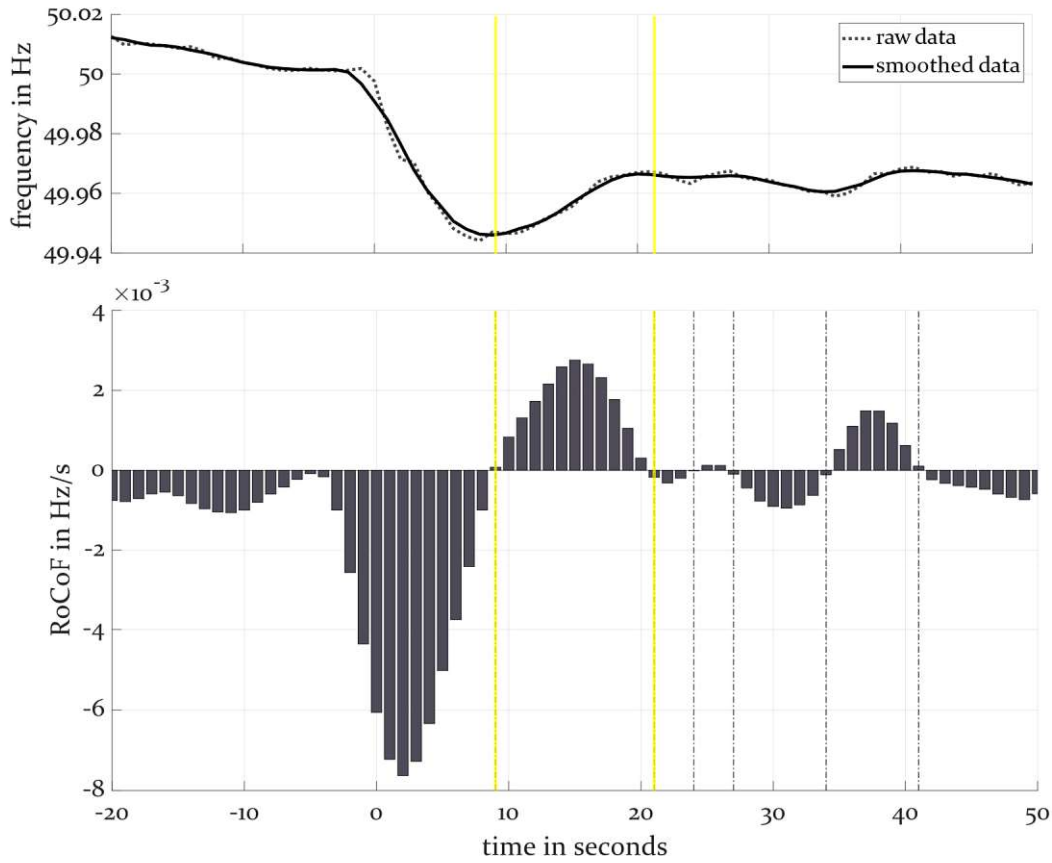


Figure 28: RoCoF detection and selection

For the further calculations, the first two detected RoCoF-zero-crossing points after the event start are used (marked in yellow).

4.2.3 Mathematical formulation of the RoCoF zero crossing method

The basic power balance equation for the method is:

$$\Delta P(t) + P_{SRE}(t) + P_{FCR}(t) = \Delta P_{\Sigma}(t) \quad 4.4$$

with

$$\Delta P(t) = P_G - P_L : \text{ power imbalance (generation - load) } \Delta P(t) = \begin{cases} 0 & t < t_0 \\ \Delta P & t \geq t_0 \end{cases},$$

$P_{SRE}(t)$: SRE,
 $P_{FCR}(t)$: power of the activated primary control,
 $\Delta P_{\Sigma}(t)$: overall power imbalance.

The resulting RoCoF is depending on the current power imbalance $\Delta P_{\Sigma}(t)$:

$$\frac{df}{dt} \approx \frac{\Delta P_{\Sigma}(t)}{P_{Sys}} \cdot \frac{f_n}{2 \cdot H_{Sys}} \quad 4.5$$

with

- P_{Sys} : total system size,
- H_{Sys} : system inertia constant,
- f_n : nominal frequency.

Equation 4.4 simplifies at all points in time when the RoCoF is zero.

$$\begin{aligned} \frac{df}{dt} = 0 &\Rightarrow \Delta P_{\Sigma}(t) = 0 \\ \Delta P(t) + P_{SRE}(t) + P_{FCR}(t) &= 0 \end{aligned} \quad 4.6$$

P_{SRE} is modeled directly proportional to the current frequency deviation ($\Delta f(t) = f(t) - f_n$) and results in:

$$P_{SRE}(t) = -\Delta f(t) \cdot P_{Sys} \cdot k_{SRE} \quad 4.7$$

The dynamics of the activated primary control P_{FCR} are considered with a dynamic factor d_{FCR} .

$$P_{FCR} = -\Delta f(t) \cdot d_{FCR}(t) \cdot K_{FCR} \quad 4.8$$

A potential over-fulfillment of FCR may be included in the estimated power system frequency characteristic K_{FCR} .

4.2.3.1 Dynamic factor d_{FCR}

To meet the minimum requirements, discussed in chapter 0, a dynamic behavior for the FCR in form of an PT1 element with a time constant T_1 of 6 seconds is used. This transfer function can be approximated numerically with the Implicit Euler method.

The equation shows the PT1 transfer function for the FCR:

$$G(s) = \frac{y(s)}{u(s)} = \frac{K_{FCR}}{1 + sT_1} = \frac{\frac{K_{FCR}}{T_1}}{s + \frac{1}{T_1}} \quad 4.9$$

$$y(s) \cdot \left(s + \frac{1}{T_1} \right) = \frac{K_{FCR}}{T_1} \cdot u(s)$$

$$y(s) \cdot s + \frac{y(s)}{T_1} = \frac{K_{FCR}}{T_1} \cdot u(s) \quad 4.10$$

The equation 4.10 is transformed via inverse Laplace transformation to:

$$\dot{y}(t) + \frac{y(t)}{T_1} = \frac{K_{FCR}}{T_1} \cdot u(t) \quad 4.11$$

This differential equation can be numerically approximated, with k as iteration step, to:

$$\frac{y_k - y_{k-1}}{\Delta t} + \frac{1}{T_1} \cdot y_k = \frac{K_{FCR}}{T_1} \cdot u_k \quad 4.12$$

The equation 4.12 is rearranged to y_k and simplified:

$$y_k = y_{k-1} + \frac{\Delta t}{T_1 + \Delta t} \cdot (K_{FCR} \cdot u_k - y_{k-1}) \quad 4.13$$

Using for the input u the frequency deviation Δf and for the output y the power provided from the FCR (P_{FCR}) the final equation is obtained:

$$P_{FCR}(k) = P_{FCR}(k-1) + \frac{\Delta t}{T_1 + \Delta t} \cdot (K_{FCR} \cdot \Delta f(k) - P_{FCR}(k-1)) \quad 4.14$$

Equation 4.14 can now be divided by K_{FCR} to obtain the dynamic factor d_{FCR} .

$$d_{FCR}(k) = d_{FCR}(k-1) + \frac{\Delta t}{T_1 + \Delta t} \cdot (\Delta f(k) - d_{FCR}(k-1)) \quad 4.15$$

The dynamic factor $d_{FCR}(k)$ is depending on the previous dynamic factor $d_{FCR}(k-1)$. Thus, this factor can only be determined iteratively with known frequency deviation Δf in each step.

4.2.3.2 Solving the equation system

The linear equation system is established if equation 4.6 is set up for the first two RoCoF zero points in time (t_1, t_2) after the incident.

$$\Delta P + P_{SRE}(t_1) + P_{FCR}(t_1) = 0 \quad 4.16$$

$$\Delta P + P_{SRE}(t_2) + P_{FCR}(t_2) = 0$$

With the Equation 4.7 and 4.8 the linear equation system with two unknown parameters (k_{SRE}, K_{FCR}) is established and can be solved.

$$\Delta P - \Delta f(t_1) \cdot P_{Sys} \cdot \mathbf{k}_{SRE} - \Delta f(t_1) \cdot d_{FCR}(t_1) \cdot \mathbf{K}_{FCR} = 0 \quad 4.17$$

$$\Delta P - \Delta f(t_2) \cdot P_{Sys} \cdot \mathbf{k}_{SRE} - \Delta f(t_2) \cdot d_{FCR}(t_2) \cdot \mathbf{K}_{FCR} = 0$$

4.3 Fix supporting points method

The fix supporting points method is similar to the previously described RoCoF zero crossing method. However, two fix supporting points, one at 10 seconds (t_1) and the other at 30 seconds (t_2), are used. Since the RoCoF might not be zero at the two supporting points, the inertial response additionally needs to be considered in the power balance. The occurred power imbalance ΔP is compensated by the reaction of the SRE (P_{SRE}), the activation of the FCR (P_{FCR}) and the inertial response of the synchronous machines (ΔP_{Σ}). Figure 29 depicts the components of the model and the sum of the components (dotted line). The factors (K_{FCR} , k_{SRE}) are chosen in a way that the sum of FCR, SRE and inertial response returns exactly the imbalance ΔP (solid line) at the fixed supporting points (t_1, t_2).

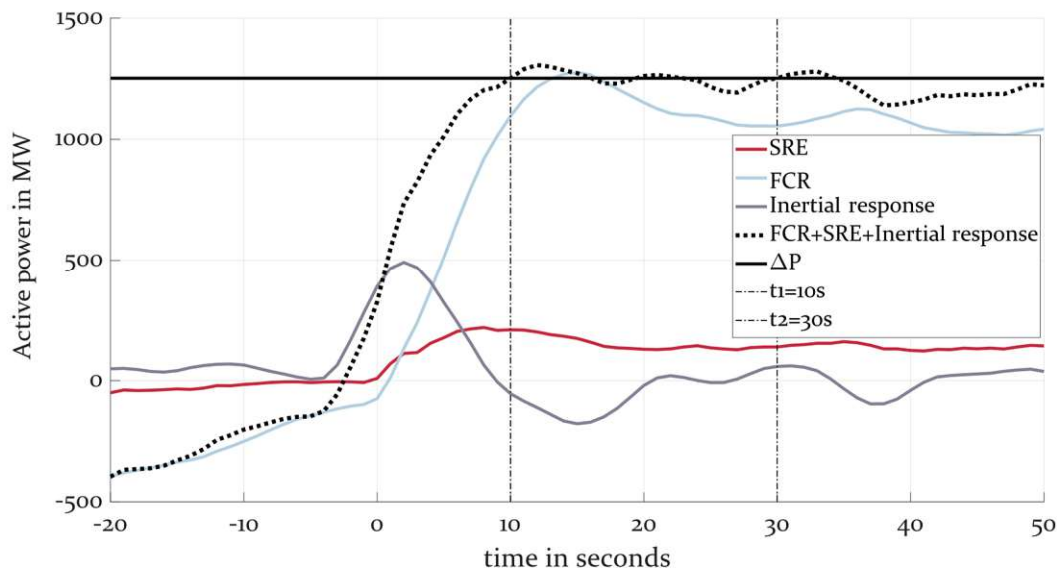


Figure 29: Fix supporting point method for 21.08.2017-event

To calculate the inertial response, equation 4.5 is used and rearranged on ΔP_{Σ} :

$$\Delta P_{\Sigma} \approx \frac{df}{dt} \cdot \frac{P_{sys} \cdot 2 \cdot H_{sys}}{f_n} \quad 4.18$$

For the further calculation a smoothed RoCoF $\frac{d\bar{f}}{dt}$ is introduced:

$$\Delta P_{\Sigma} \approx \frac{d\bar{f}}{dt} \cdot \frac{P_{sys} \cdot 2 \cdot H_{sys}}{f_n} \quad 4.19$$

The same basic power balance equation as for the previous method is used:

$$\Delta P(t) + P_{SRE}(t) + P_{FCR}(t) = \Delta P_{\Sigma}(t) \quad 4.20$$

The equations for P_{SRE} , P_{FCR} and dynamic factor d_{FCR} can be taken from the RoCoF zero crossing method.

The linear equation system can be established if equation 4.20 is set up for the fixed points in time (t_1, t_2).

$$\Delta P + P_{SRE}(t_1) + P_{FCR}(t_1) = \Delta P_{\Sigma}(t_1) \quad 4.21$$

$$\Delta P + P_{SRE}(t_2) + P_{FCR}(t_2) = \Delta P_{\Sigma}(t_2)$$

With the Equation 4.7, 4.8 and 4.19 the linear equation system with two unknown parameters (k_{SRE}, K_{FCR}) is set up and can be solved.

$$\Delta P - \Delta f^*(t_1) \cdot P_{Sys} \cdot \mathbf{k}_{SRE} - \Delta f^*(t_1) \cdot d_{FCR}^*(t_1) \cdot \mathbf{K}_{FCR} = \frac{d\bar{f}}{dt}(t_1) \cdot \frac{P_{Sys} \cdot 2 \cdot H_{Sys}}{f_n} \quad 4.22$$

$$\Delta P - \Delta f^*(t_2) \cdot P_{Sys} \cdot \mathbf{k}_{SRE} - \Delta f^*(t_2) \cdot d_{FCR}^*(t_2) \cdot \mathbf{K}_{FCR} = \frac{d\bar{f}}{dt}(t_2) \cdot \frac{P_{Sys} \cdot 2 \cdot H_{Sys}}{f_n}$$

4.4 Optimal fit method

This method approximates the simulated system model frequency to the real frequency measurements by optimizing the relevant system parameters. The model used is shown in Figure 20 and is adjusted with a pre-existing power imbalance to consider the system state before the event. Due to this additional power imbalance, the simulated frequency starts with a pre-existing frequency deviation at the time of the incident.

In this method, the gain of the FCR reaction K_{FCR} , the SRE k_{SRE} and the system inertia constant H_{Sys} are subject to the optimization. The system inertia constant H_{Sys} is not fixed on a specified value (as in the fix supporting points method), instead it is taken as additional degree of freedom for the optimization.

4.4.1 Optimization approach

A least squared error optimization approach is applied in which the optimization variables ($K_{FCR}, k_{SRE}, H_{Sys}$) are varied such that the squared error S returns a minimum value. The mathematical notation for the optimization is:

$$\min S = \sum_{t=0}^{t_{End}} (f_{measured}(t) - f(t, \beta))^2 \quad \text{with } \beta = [K_{FCR}, k_{SRE}, H_{Sys}] \quad 4.23$$

where $f_{measured}(t)$ is the measured frequency and $f(t, \beta)$ the simulated frequency based on the optimized variables $\beta = [K_{FCR}, k_{SRE}, H_{Sys}]$.

The optimization variables can be varied in certain intervals within step sizes listed in Table 6:

Table 6: List of optimization variables with interval and step size

Variable	Units	Interval	Step size
H_{Sys}	s	4 - 25	0.5
K_{FCR}	MW/Hz	10 000 - 100 000	200
k_{SRE}	%/Hz	0 - 0.1	0.0005
t_{End}	s	20 - 35	5

Figure 30 shows the optimal fit method for an event with a 30 seconds optimization interval. All different combinations of $K_{FCR}, k_{SRE}, H_{Sys}$ are calculated and the setting with the lowest squared error is chosen.

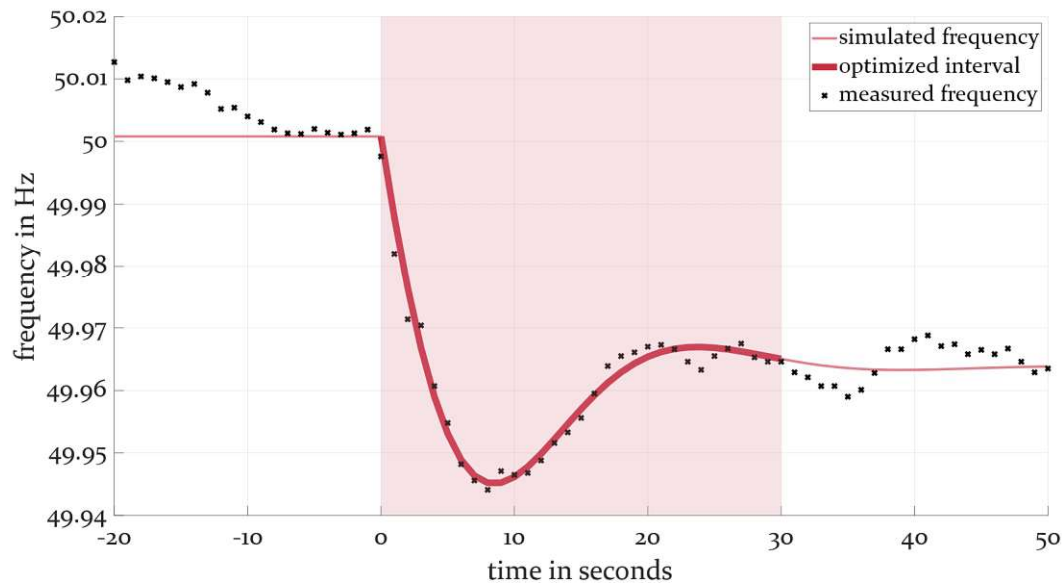


Figure 30: Optimal fit method with 30 seconds interval for 21.08.2017-event

The calculation is performed for different optimization interval sizes within the range of 20 to 35 seconds after the event.

5 Results

In the following chapters, the estimated values of the SRE k_{SRE} and the power system frequency characteristic of the Frequency Containment Reserve K_{FCR} for all events and methods applied are analyzed and compared. The detailed results of this analysis can be found in Annex B. A GUI (Graphical User Interface) was developed for a quick visualization of the results. This GUI will not be discussed in detail in this thesis, but a screenshot can be seen in Annex A.

5.1 RoCoF zero crossing method

The results of the RoCoF zero crossing method are strongly dependent on the detected RoCoF zero crossing supporting points. For an exemplary event shown in Figure 26, a plausible value of 1.72 %/Hz for k_{SRE} and 28.46 GW/Hz for K_{FCR} is found. However, the analysis of all events, depicted in Figure 31, shows a rather wide range of values for k_{SRE} . The grey bars show the chronological results and the solid black line shows the duration curve. Nearly half of the identified values for k_{SRE} are negative and thus implausible. This also leads to an unsatisfactory mean value of -1.11 %/Hz and a low median value of 0.9 %/Hz.

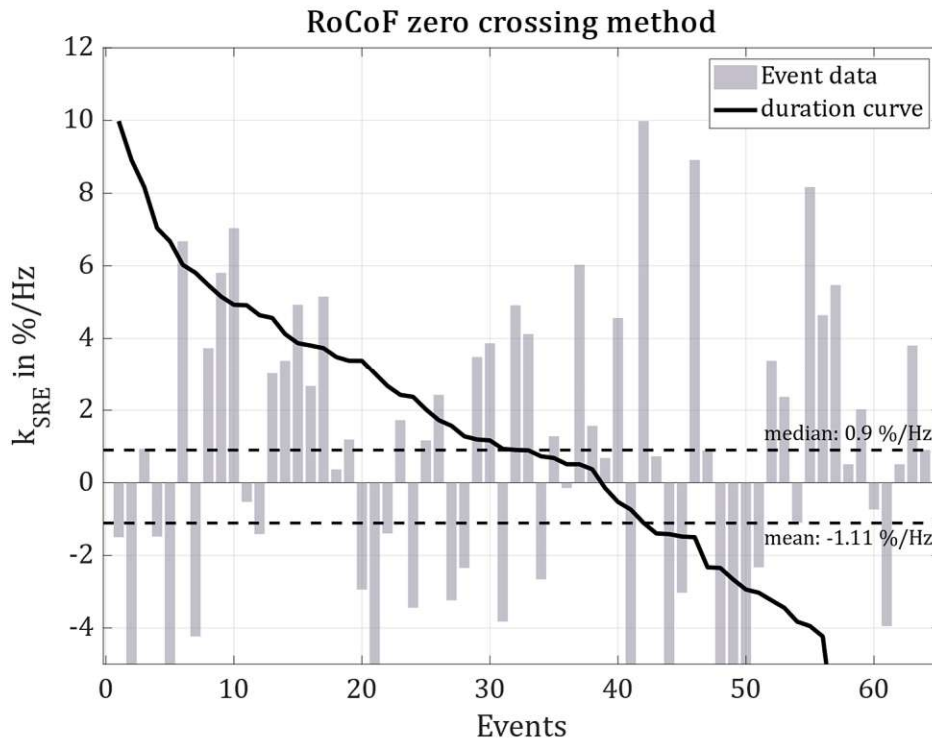


Figure 31: Range of k_{SRE} -values with RoCoF zero crossing method

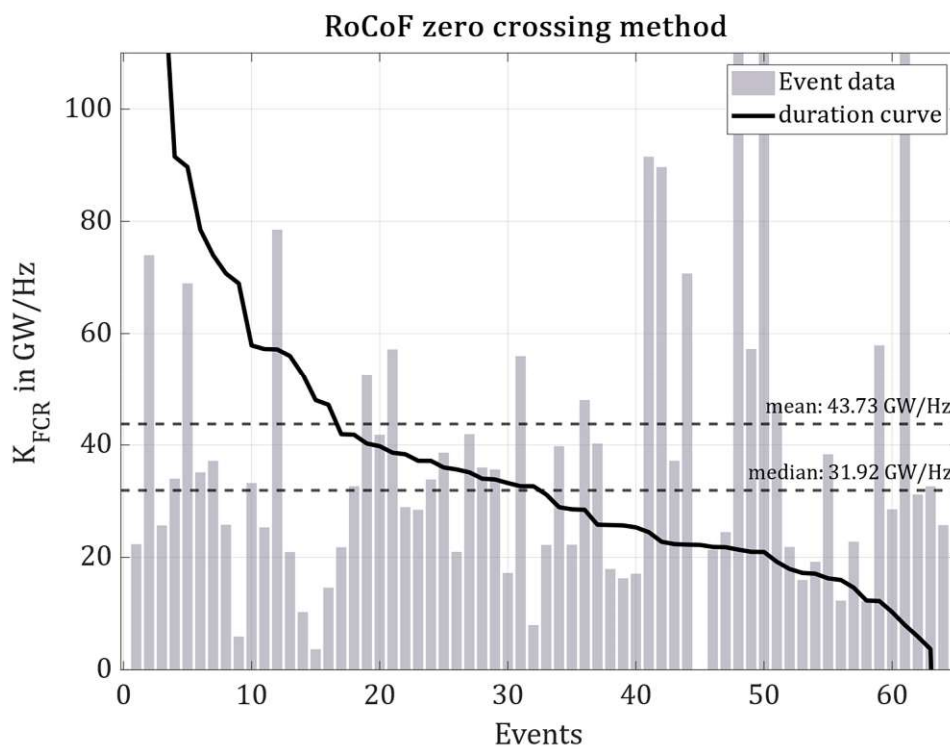


Figure 32: Range of K_{FCR} -values with RoCoF zero crossing method

The K-factor of the FCR, depicted in Figure 32, shows unrealistically high K_{FCR} -values, as a result of the simplified linear equation system approach. These high values lead to a mean of 43.73 GW/Hz. The median holds a rather realistic value of 31.92 GW/Hz. The resulting power system frequency characteristic (K_{Grid}) is composed of the FCR K-factor and the SRE K-factor.

It is noticeable that the estimated shares of K_{FCR} relatively often exceed the value equal to 15 GW/Hz (dashed line in Figure 33). Hence, a significant over-fulfillment of the FCR can be identified. Moreover, a strong negative correlation can be seen between unrealistically high K_{FCR} -values and negative values of k_{SRE} .

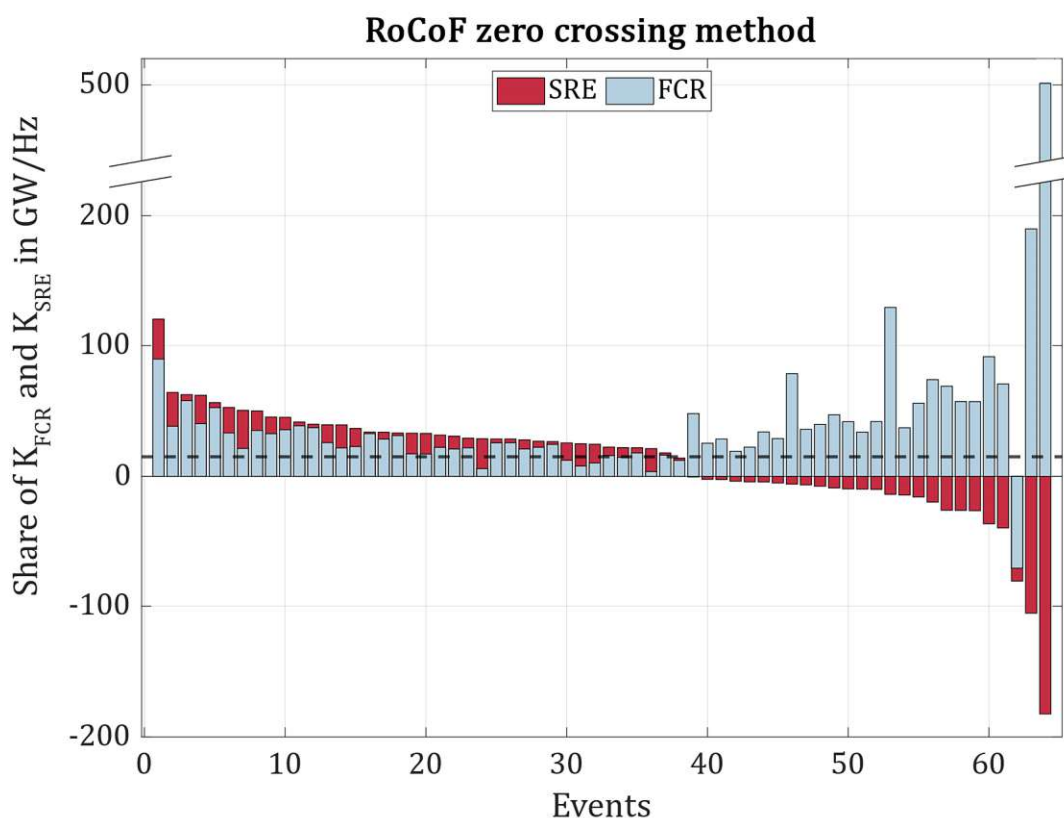


Figure 33: Composition of K_{Grid} with RoCoF zero crossing method

The results of this method are not acceptable for a proper identification of the SRE. The solution of the linear equation system is depending on the dynamic factor d_{FCR} and the measured frequency deviation Δf . The measured frequency values were provided at a resolution of 1 second, which might be insufficient for properly investigating the dynamic behavior of a power system. Taking this into account, the detection of the RoCoF zero crossing supporting points is not obvious and a supporting point shift by just one second may already significantly change the result of the equation system.

5.2 Fix supporting points method

To reduce the susceptibility of errors, an alternative approach with fix supporting points seems reasonable. Fix supporting points improve the repeatability. For a specific event shown in Figure 29, a plausible value of 1.27 %/Hz for k_{SRE} and a value of 33.68 GW/Hz for K_{FCR} is found. This method identifies less negative k_{SRE} -values than the RoCoF zero crossing method. However, the results of the fix supporting points method, depicted in Figure 34, still show a wide range of the SRE with a mean value of 5.32 %/Hz and a median value of 2.57 %/Hz.

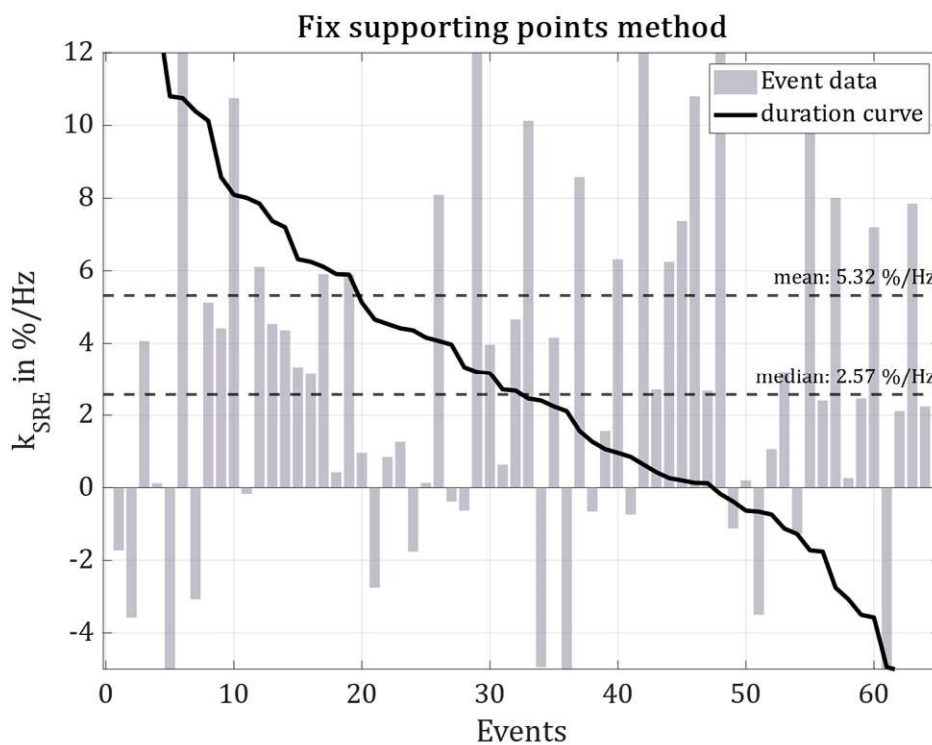


Figure 34: Range of k_{SRE} -values with fix supporting points method

For the K-factor of the FCR the mean value is 18.57 GW/Hz and the median holds a value of 22.85 MW/Hz.

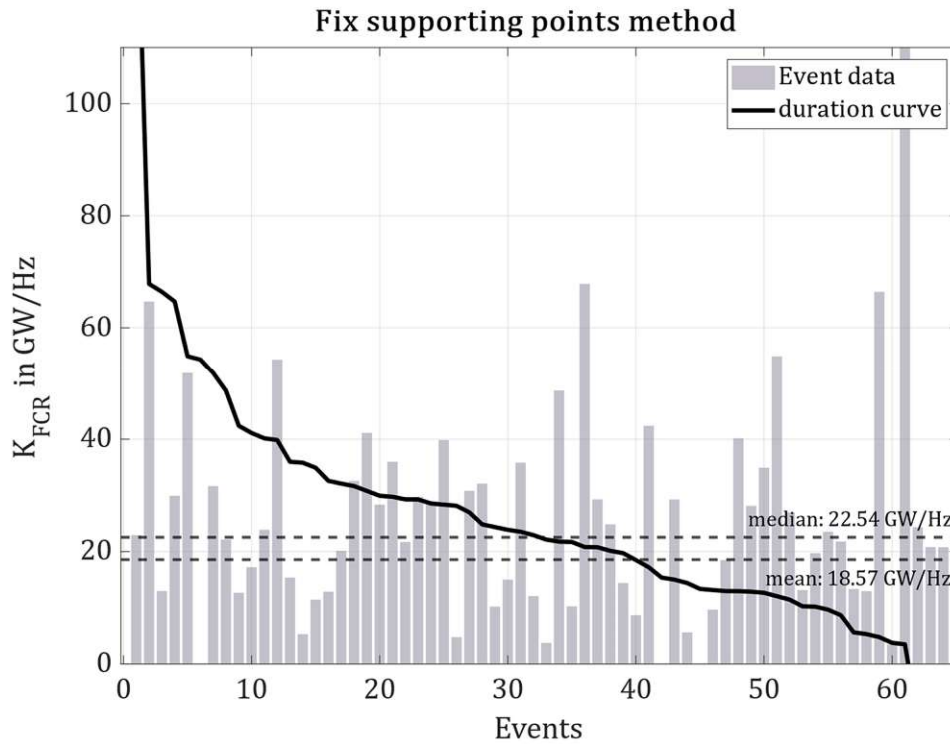


Figure 35: Range of K_{FCR} -values with fix supporting points method

As can be seen in Figure 36 this method generally decomposes the K_{Grid} into a larger share of SRE than the RoCoF zero crossing method does. This hypothesis can be accentuated with a comparison of the K_{FCR} and k_{SRE} mean or median values.

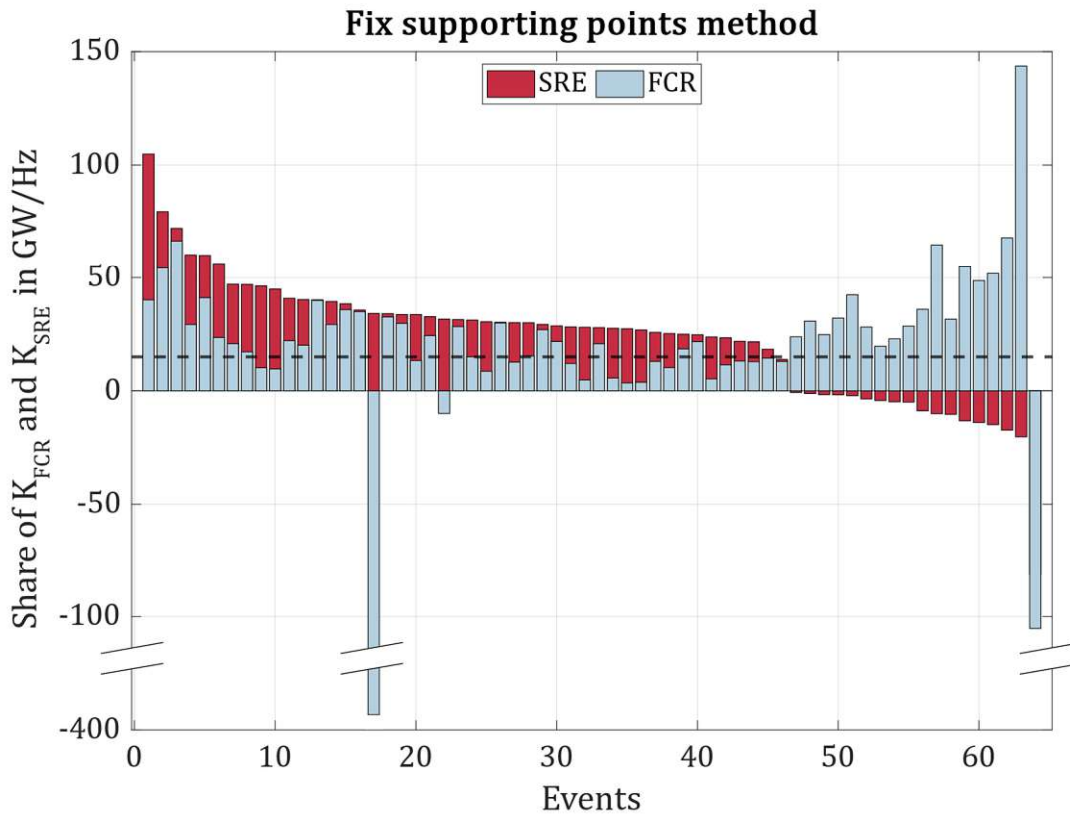


Figure 36: Composition of K_{Grid} with fix supporting points method

For some events, the SRE share holds over two thirds of K_{Grid} . A strong negative correlation between unrealistically high K_{FCR} -value and negative k_{SRE} can be again observed. Similar to the RoCoF zero crossing method the results of this method are not acceptable for a proper identification of the SRE.

5.3 Optimal fit method

Compared to the previously discussed methods, the optimal fit method still returns a wide range of k_{SRE} -values, but most of the results seem plausible. It should be noted, however, that for some events the limits of the parameter optimization prevented larger outliers. Figure 37 shows the range of the k_{SRE} results.

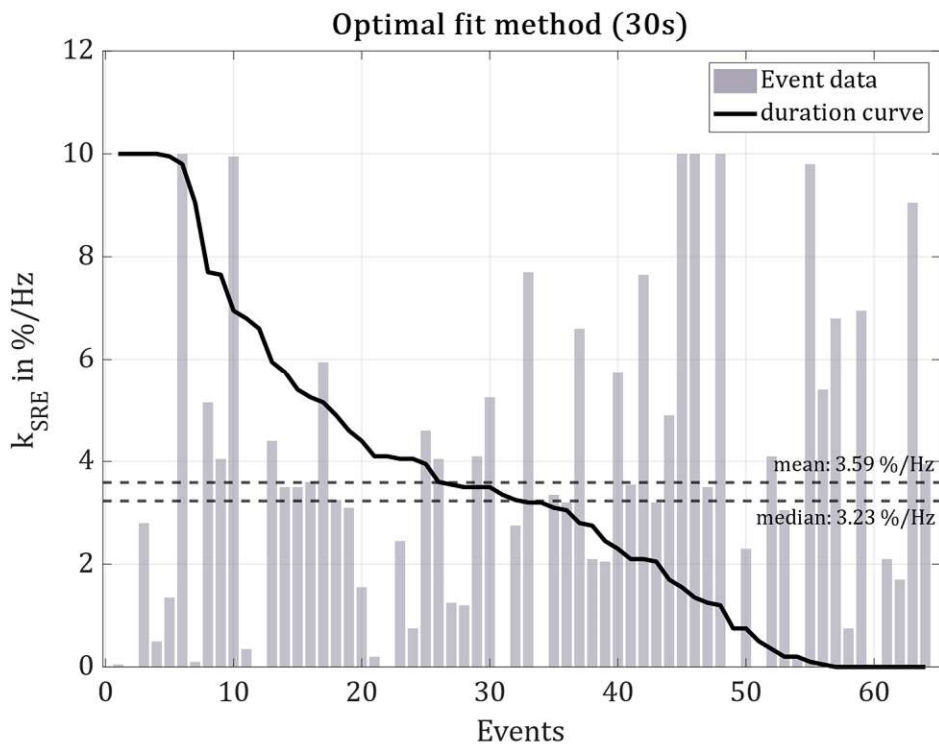


Figure 37: Range of k_{SRE} -values with optimal fit method (30 seconds)

Except for three events, the optimized K_{FCR} is lower than 50 GW/Hz, shown in Figure 38. The mean value exceeds 1.7 times the expected reaction of FCR (15 GW/Hz).

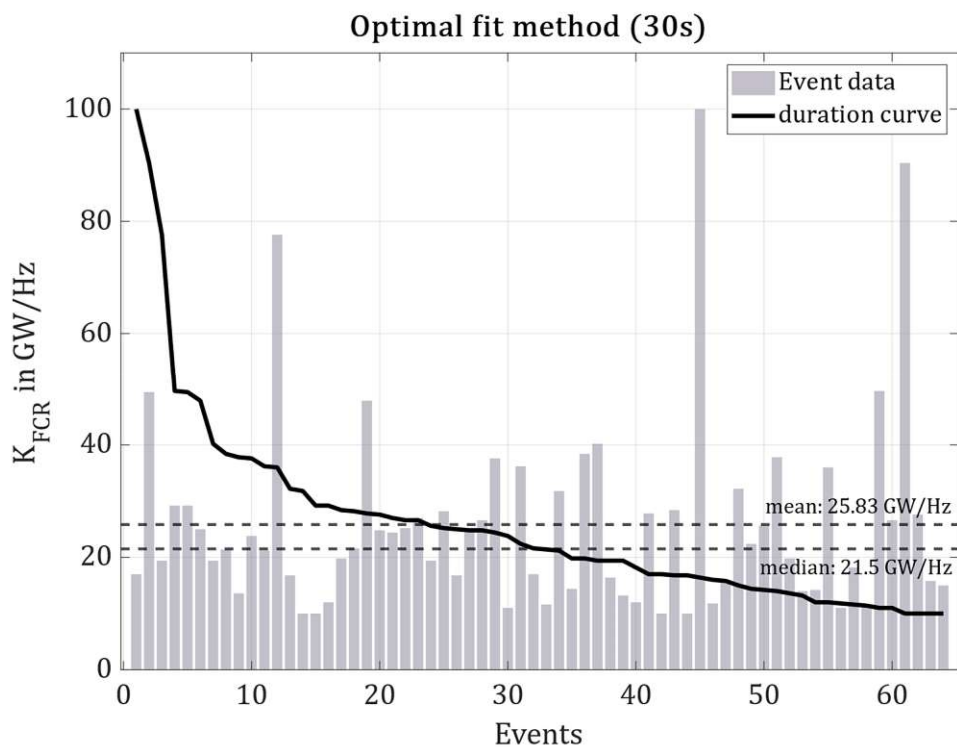


Figure 38: Range of K_{FCR} -values with optimal fit method (30 seconds)

Compared with the expected FCR reaction, an under-fulfillment occurs in 25 % of the events. This under-fulfillment typically correlates with a relatively large SRE, as shown in Figure 39.

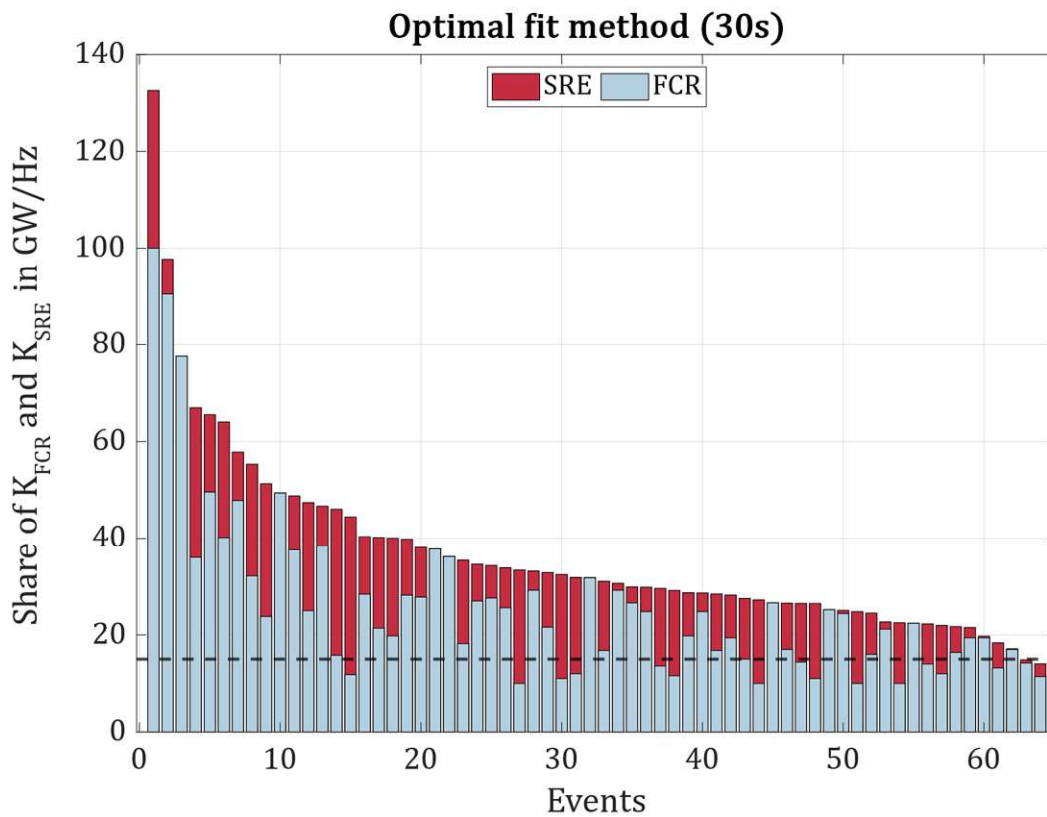


Figure 39: Composition of K_{Grid} with optimal fit method (30 seconds)

As mentioned in Table 6, the end of the optimization interval t_{End} can be varied. The least squared error optimization finds different optimal system parameters for various interval lengths. A comparison of the K_{Grid} results for a 30 and 20 seconds optimization interval is shown in Figure 40.

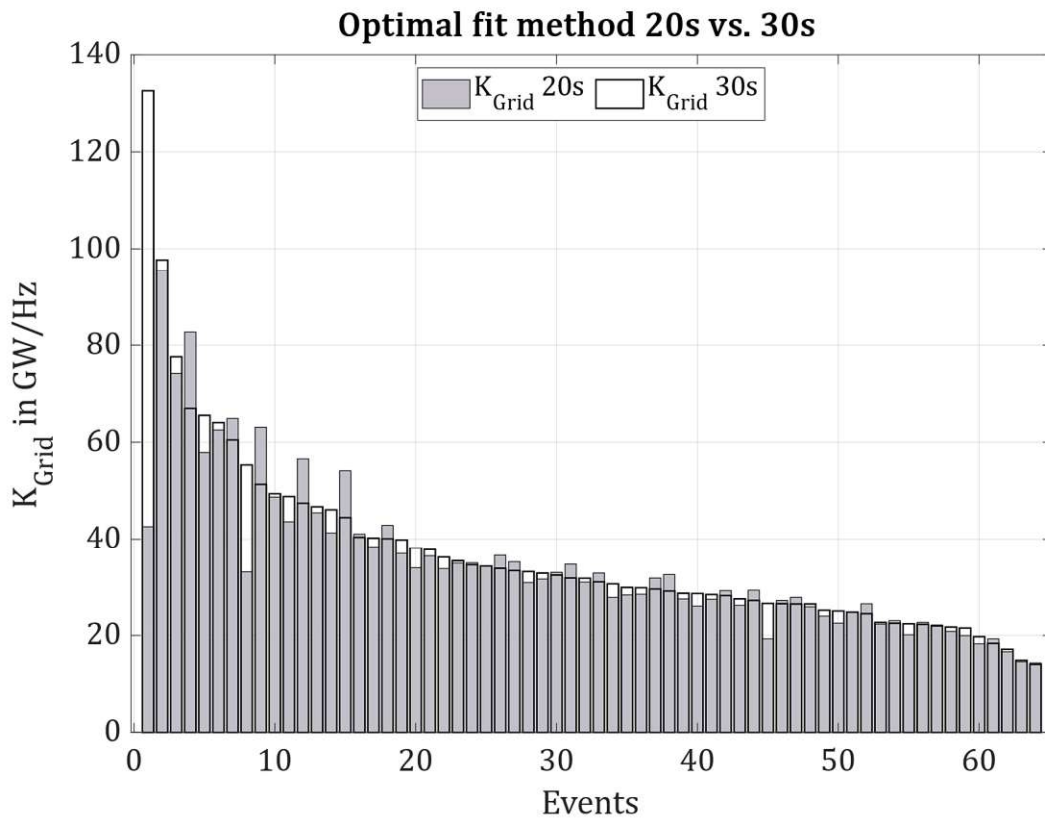


Figure 40: Comparison of K_{Grid} for optimal fit interval length 30 and 20 seconds

For more than the half of the events, a 30 seconds optimization interval results in a higher K_{Grid} value as for a 20 seconds optimization interval. This difference is also explained in Figure 41 and Figure 42. It is noticeable that the estimated SRE is more likely to influence the simulated frequency nadir depth, while the value of K_{FCR} more affects the quasi-steady-state frequency deviation. For smaller optimization intervals, the simulation represents the depth of the nadir more accurate, which results in slightly larger K_{SRE} values. For larger optimization intervals, the simulation represents the quasi-steady-state deviation more precise, and thus slightly larger K_{FCR} values are obtained.

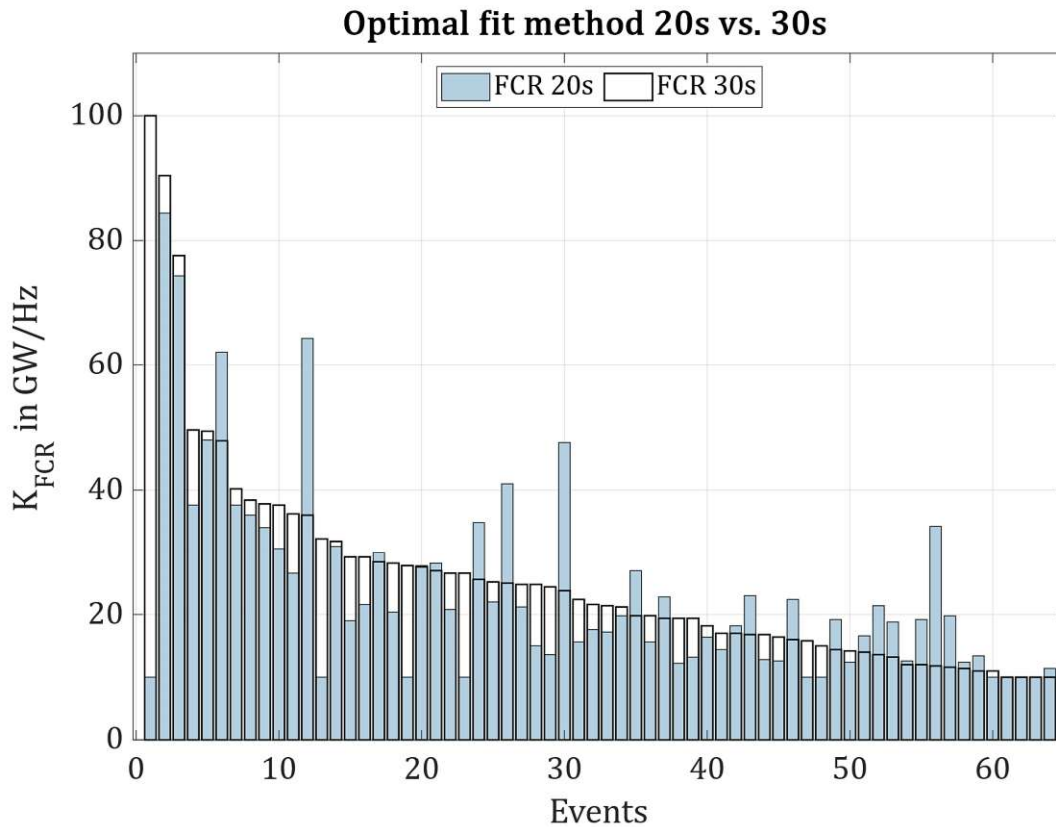


Figure 41: Comparison of K_{FCR} for optimal fit interval length 30 and 20 seconds

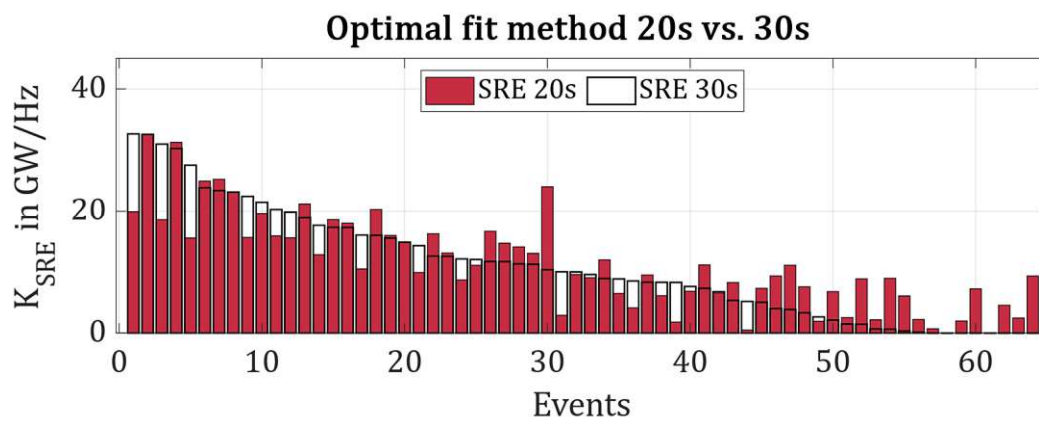


Figure 42: Comparison of K_{SRE} for optimal fit interval length 30 and 20 seconds

Summarized, it can be concluded that the optimal fit method generates plausible values for all chosen optimization interval lengths. Compared to the other methods, the Optimal fit method performs more robust for the various frequency events. The results from this method have therefore been used for a further statistical analysis.

5.4 Comparison between the methods

As already shown in the previous chapters it is impossible to obtain comparable average values for the SRE for each method, due to a high amount of outliers. A new approach is therefore used to achieve comparability between the methods. The total power system frequency characteristic is composed of a part depending on the system size K_{SRE} and a part independent of the system size (K_{FCR}), as shown in equation below.

$$K_{Grid} = K_{FCR} + K_{SRE} = \mathbf{K}_{FCR} + \mathbf{k}_{SRE} \cdot P_{Sys} \quad 5.1$$

With this dependency a linear regression of $K_{Grid}(P_{Sys})$ can be performed to obtain an average value for k_{SRE} and K_{FCR} . Figure 43 shows the linear regressions and Table 7 gives a summary of the previous results in comparison with the new linear regression approach for all methods.

Table 7: Results of the average calculations and the linear regression calculations

Method	Average values		Linear regression values	
	k_{SRE} in %/Hz	K_{FCR} In MW/Hz	k_{SRE} in %/Hz	K_{FCR} In GW/Hz
RoCoF zero crossing	-1.11	43.73	-13.12	82.50
Fix supporting points	5.32	18.57	-1.71	40.16
Optimal fit - 20 s interval	3.72	23.77	1.31	30.97
Optimal fit - 25 s interval	3.67	25.45	0.99	33.53
Optimal fit - 30 s interval	3.59	25.83	0.92	33.84
Optimal fit - 35 s interval	3.48	26.24	0.82	34.24

As can be seen in Table 7 the RoCoF zero crossing and Fix supporting points method provide implausible negative SRE values. The optimal fit method for all intervals show plausible, but quite low SRE-values. Therefore, the results of the optimal fit method with an optimization interval of 30 seconds are used for further statistical analysis. The 30 seconds interval is preferred, because this time span covers exactly the full activation of FCR.

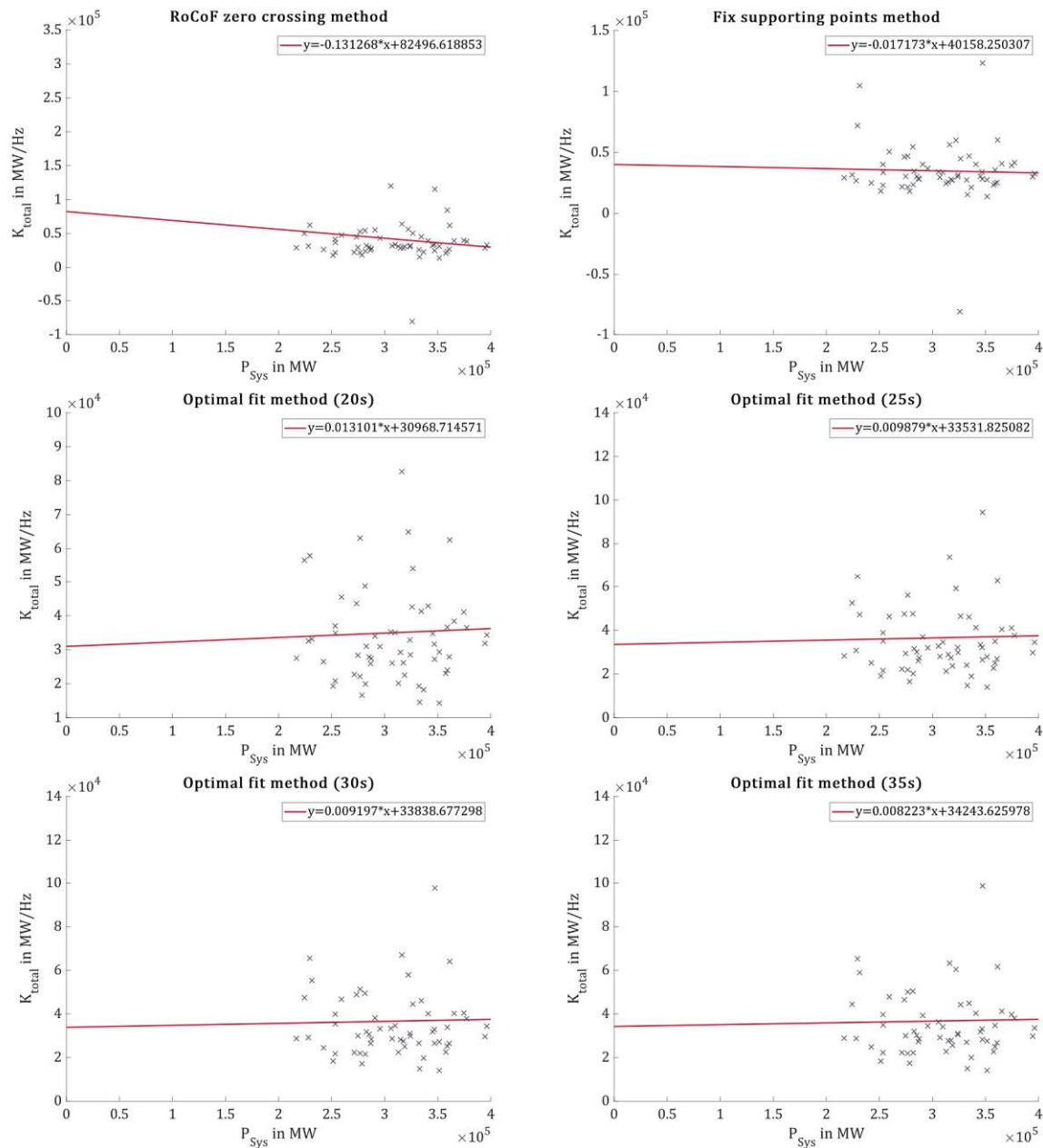


Figure 43: Comparison of the decomposition of the K-factor

5.5 Statistical analysis

This chapter analyzes whether it is possible to find daily, weekly and seasonal patterns or correlations between the SRE and other operational conditions such as the system size.

For the following figures the results of the 30 seconds – optimal fit method are used to observe this patterns or correlations. Neither a correlation between the k_{SRE} and the season of the year

nor the day of the week is found. Also, no correlation between the k_{SRE} and the time of the day can be found.

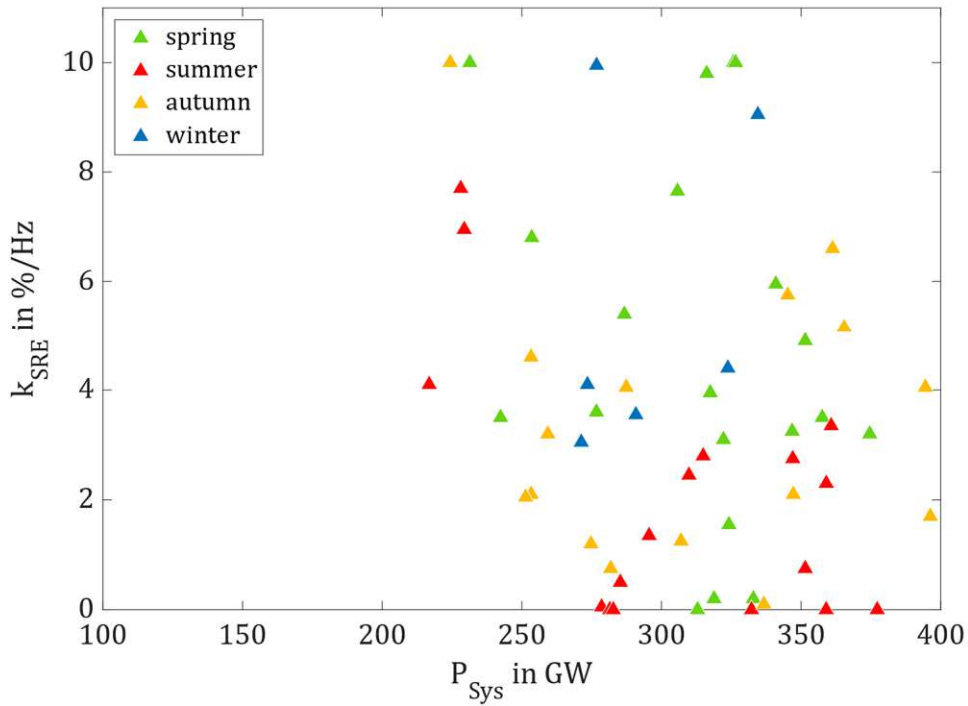


Figure 44: Correlation of k_{SRE} and season

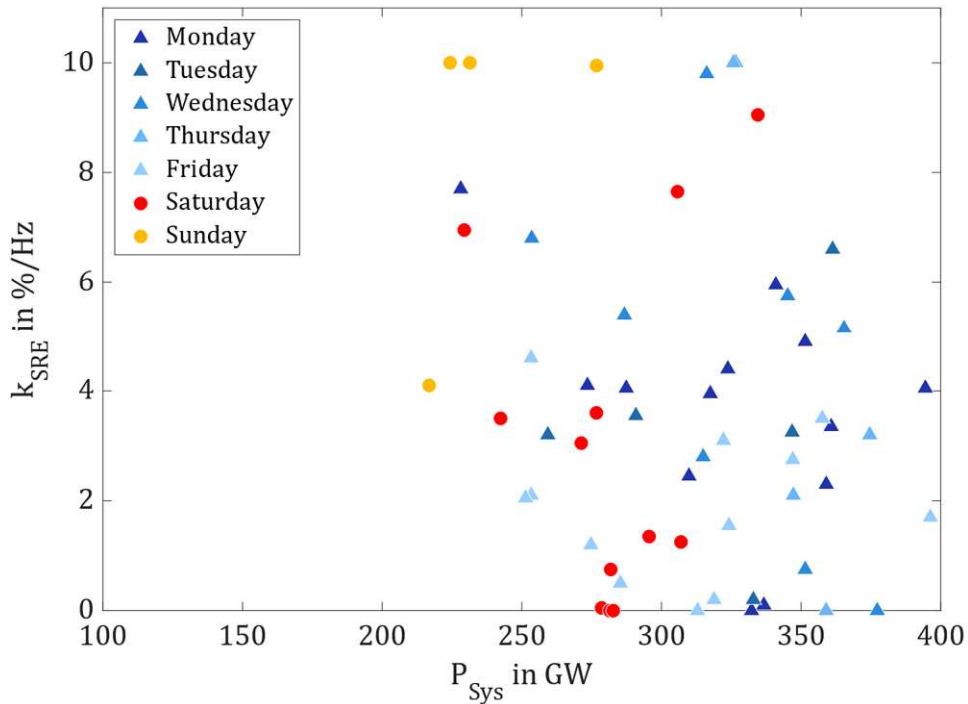


Figure 45: Correlation of k_{SRE} and day of the week

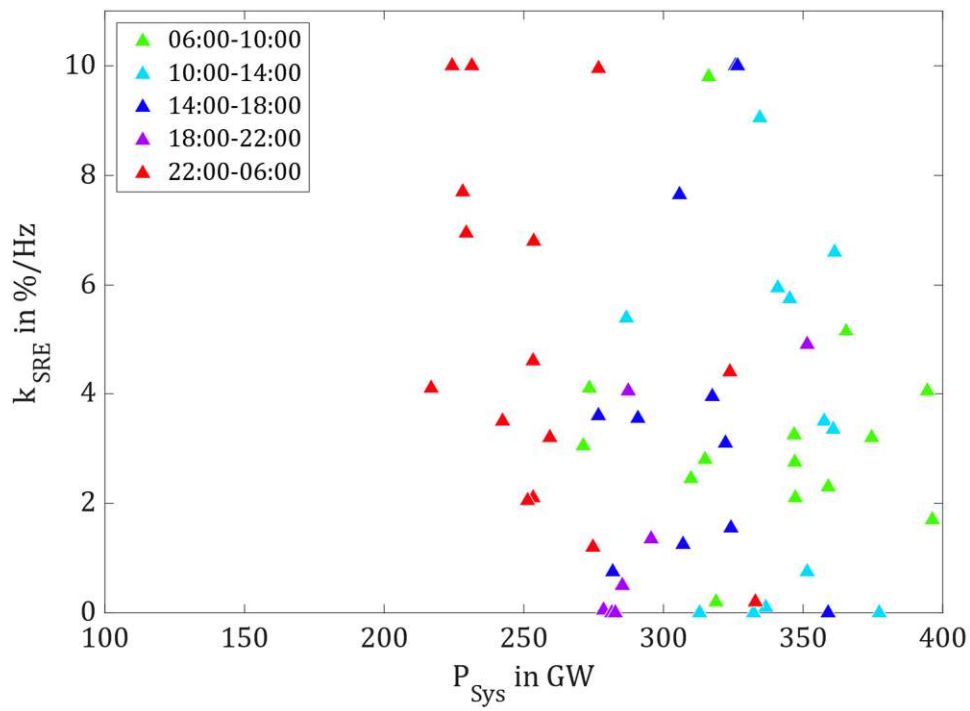


Figure 46: Correlation of k_{SRE} and time of the day

6 Conclusion

A reliable SRE value is crucial for accurate modelling of the system frequency response to a power imbalance. Therefore, data of 64 frequency events were used to identify the SRE and the composition of the K-factor. The investigation is performed using a top-down approach with three different methods. This approach shows a wide range for k_{SRE} and K_{FCR} among the different methods used.

The RoCoF zero crossing method does not need any assumptions of the system inertia constant and is thus a rather simple method, which also considers the dynamics in the frequency time series. However, it has been shown that particularly with low resolution frequency measurements these potential advantages come along in many events with obviously unfeasible (negative) values. The RoCoF zero crossing method is therefore not recommended for a future use.

The fix supporting points method increases robustness but loses simplicity since the system inertia constant needs to be additionally preprocessed. With this method, the distribution of results is reduced, but it still does not provide feasible values and thus its use is also not recommended.

The optimal fit method can describe the frequency deviation and the dynamics of the provided events best with the identified system parameters. Different optimization intervals were investigated and similar plausible values for k_{SRE} (0.8 - 1.3 %/Hz) and K_{FCR} (30.9 - 34.2 GW/Hz) were obtained. The composition of K_{Grid} and their values slightly change depending on the interval length.

The decomposition of the power system frequency characteristic K-factor strongly depends on the dynamics of the main influencing components. In this thesis, k_{SRE} is directly proportional to the frequency deviation Δf and K_{FCR} directly proportional to Δf with a dynamic lag (PTI

behavior). This is a simple approach of describing a complex response mechanism and may not perfectly match the reality.

Within this thesis it has also been shown that the overall K-factor is typically higher compared to the Design Hypothesis of the CE power system. Its composition varies depending on the method used. This can be explained by an over-fulfillment of the FCR and a potentially higher SRE.

The reason of the wide range of results may be explained with following factors:

- The basic model used in this thesis consists of a single node system to describe the entire CE power system. This approach uses a simple and possibly not completely accurate dynamics for the FCR and SRE.
- Instead of the hypothetical frequency response at the Center of Inertia (COI), the frequency measurements at a substation close to Vienna were used.
- Due to lack of information on the dynamic of the power imbalance, a simple step function has been used.

Finally, a k_{SRE} larger than 1 %/Hz can be confirmed but there is a strong need of accurate monitoring of FCR activation to determine the k_{SRE} more precisely. Furthermore, no decrease of the k_{SRE} within the analyzed time interval of the events was found. Moreover, no patterns or correlations of the SRE with season, day of the week and time of the day have been identified.

LIST OF FIGURES

Figure 1: Classification of power system stability. Adapted from [5]	3
Figure 2: Balance between generation and load	4
Figure 3: Kinetic energy of CE [7]	8
Figure 4: ASM and working machine behavior. Adapted from [3]	9
Figure 5: Activation of load-frequency control. Adapted from [11]	12
Figure 6: Primary control characteristic.....	13
Figure 7: Operation point. Adapted from [12]	13
Figure 8: Dynamic options of FCR	14
Figure 9: Design Hypothesis according UCTE. Adapted from [6]	15
Figure 10: Dynamic and quasi-steady-state deviation. Adapted from [6]	16
Figure 11: Methodology for K-factor calculation	17
Figure 12: Sample for the Austrian LFDD-plan [15]	20
Figure 13: Scheme of LFSM-O behavior [16].....	20
Figure 14: Block diagram of the balancing model.....	21
Figure 15: Block diagram of Inertial response behavior.....	22
Figure 16: Block diagram of SRE	23
Figure 17: Block Diagram for primary control.....	23
Figure 18: FCR, SRE-reaction to a power imbalance with resulting frequency deviation	24
Figure 19: Overview of the methodology approach	26
Figure 20: Simulation model with known (yellow) and unknown (red, blue) parameters	27
Figure 21: Events per timeslot per day.....	28
Figure 22: frequency measurements at 21.08.2017 – 06:50	29
Figure 23: Map of Regional Group Continental Europe	30
Figure 24: Calculated CE system load profile from 2016 to mid 2021	31
Figure 25: Calculated inertia profile from 2016 to mid 2021.....	33
Figure 26: RoCoF zero crossing method for 21.08.2017-event.....	34
Figure 27: Smooth function applied on raw data	35
Figure 28: RoCoF detection and selection	36
Figure 29: Fix supporting point method for 21.08.2017-event.....	40
Figure 30: Optimal fit method with 30 seconds interval for 21.08.2017-event.....	43
Figure 31: Range of $kSRE$ -values with RoCoF zero crossing method.....	45
Figure 32: Range of $KFCR$ -values with RoCoF zero crossing method	45

Figure 33: Composition of <i>KGrid</i> with RoCoF zero crossing method	46
Figure 34: Range of <i>kSRE</i> -values with fix supporting points method	47
Figure 35: Range of <i>KFCR</i> -values with fix supporting points method.....	48
Figure 36: Composition of <i>KGrid</i> with fix supporting points method	49
Figure 37: Range of <i>kSRE</i> -values with optimal fit method (30 seconds)	50
Figure 38: Range of <i>KFCR</i> -values with optimal fit method (30 seconds)	50
Figure 39: Composition of <i>KGrid</i> with optimal fit method (30 seconds)	51
Figure 40: Comparison of <i>KGrid</i> for optimal fit interval length 30 and 20 seconds.....	52
Figure 41: Comparison of <i>KFCR</i> for optimal fit interval length 30 and 20 seconds	53
Figure 42: Comparison of <i>KSRE</i> for optimal fit interval length 30 and 20 seconds.....	53
Figure 43: Comparison of the decomposition of the K-factor.....	55
Figure 44: Correlation of <i>kSRE</i> and season	56
Figure 45: Correlation of <i>kSRE</i> and day of the week.....	56
Figure 46: Correlation of <i>kSRE</i> and time of the day.....	57

LIST OF TABLES

Table 1: Classes of load torques. Adapted from [9].....	10
Table 2: $kLoad$ per technology and examples. Adapted from [10]	10
Table 3: FCR properties in different synchronous areas. Adapted from [13].....	13
Table 4: Event distribution by year	28
Table 5: Inertia constant and loading factors per production type. Adapted from [7]	32
Table 6: List of optimization variables with interval and step size.....	42
Table 7: Results of the average calculations and the linear regression calculations	54

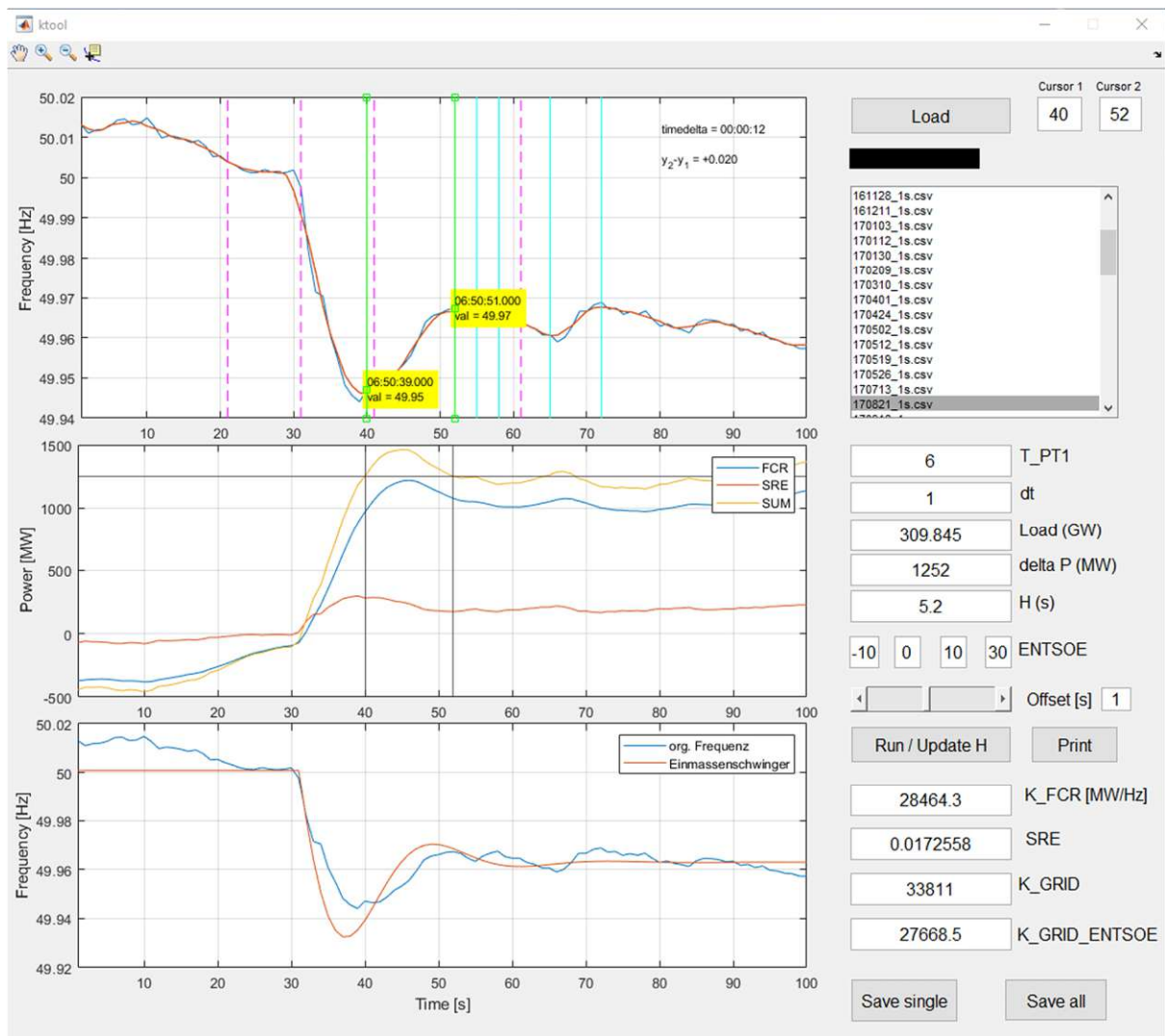
LIST OF REFERENCES

- [1] ENTSO-E, “High Penetration of Power Electronic Interfaced Power Sources,” 2017. Accessed: Jan. 24, 2022. [Online]. Available: https://eepublicdownloads.entsoe.eu/clean-documents/Publications/SOC/High_Penetration_of_Power_Electronic_Interfaced_Power_Sources_and_the_Potential_Contribution_of_Grid_Forming_Converters.pdf
- [2] S. Khan, B. Bletterie, A. Anta, and W. Gawlik, “On Small Signal Frequency Stability under Virtual Inertia and the Role of PLLs,” *Energies*, vol. 11, 2018.
- [3] E. Welfonder, H. Lens, and C. Schöll, “Bedeutung des Netzselbstregeleffekts,” *EW - Netze + Infrastruktur*, Stuttgart, pp. 46–55, 2018.
- [4] B. Ingelsson, P.-O. Lindstrom, D. Karlsson, G. Runvik, and J.-O. Sjodin, “Wide-area protection against voltage collapse,” *IEEE computer applications in power*, vol. 10, no. 4, pp. 30–35, 1997.
- [5] ENTSO-E, “Technical background and recommendations for defence plans in the continental europe synchronous area,” 2010. Accessed: Jul. 01, 2022. [Online]. Available: https://eepublicdownloads.entsoe.eu/clean-documents/pre2015/publications/entsoe/RG_SOC_CE/RG_CE_ENTSO-E_Defence_Plan_final_2011_public.pdf
- [6] UCTE Operational Handbook, “A1-Appendix 1: Load-Frequency Control and Performance [E],” 2004.
- [7] ENTSO-E, “Inertia and Rate of Change of Frequency (RoCoF),” 2020. Accessed: Oct. 28, 2021. [Online]. Available: https://eepublicdownloads.azureedge.net/clean-documents/SOC%20documents/Inertia%20and%20RoCoF_v17_clean.pdf
- [8] A. J. Schwab, *Elektroenergiesysteme*, 6. Edition. Karlsruhe: Springer Vieweg, 2020.
- [9] T. Weißbach and G. Scheffknecht, “Netzdynamikverhalten und die Rolle des Netzselbstregeleffekts,” Stuttgart, 2009. Accessed: Oct. 28, 2021. [Online]. Available: https://www.iee.tu-clausthal.de/fileadmin/downloads/07-Tobias_Weissbach.pdf
- [10] O. Brückl, M. Haslbeck, M. Riederer, C. Adelt, and J. Eller, “Zukünftige Bereitstellung von Blindleistung und anderen Maßnahmen für die Netzsicherheit,” Waldmünchen, 2016.

- [11] ENTSO-E, “Supporting Document for the Network Code on Load-Frequency Control and Reserves,” 2013.
- [12] A. Stimmer, “Modul 5: Netzbetrieb,” in *Ausbildungsunterlagen APG*, 2020.
- [13] EUROPEAN COMMISSION, “COMMISSION REGULATION (EU) - establishing a guideline on electricity transmission system operation 2017/ 1485,” 2017.
- [14] APG, “Tenders for frequency containment reserve in the APG area.” Accessed: Nov. 18, 2021. [Online]. Available: <https://www.apg.at/en/markt/netzregelung/primaerregelung/ausschreibungen>
- [15] ÖE/ Experten Pool Defence Plan, “Systemschutzplan Österreich,” 2021.
- [16] E-Control, “Technische und organisatorische Regeln für Betreiber und Benutzer (TOR),” 2019.
- [17] “ENTSO-E Transparency Platform.” <https://transparency.entsoe.eu/> (accessed Oct. 31, 2021).
- [18] “Turkish Electricity Transmission Corporation.” <https://www.teias.gov.tr/en-US> (accessed Oct. 06, 2021).

ANNEX

A Graphical User Interface



B Table of the results

Event information					RoCof zero crossing method		Fix supporting points method		Optimal fit method with 30s interval			Optimal fit method with 20s interval		
Nr.	Timestamp in CET/CEST	ΔP in MW	P_{Sys} in GW	H_{Sys} in s	K_{FCR} in MW/Hz	k_{SRE} in %/Hz	K_{FCR} in MW/Hz	k_{SRE} in %/Hz	K_{FCR} in MW/Hz	k_{SRE} in %/Hz	H_{Sys} in s	K_{FCR} in MW/Hz	k_{SRE} in %/Hz	H_{Sys} in s
1	23.07.2016 22:33	-1016	278.56	5.6	22361.8	-1.50	22931.9	-1.72	17000	0.05	5.0	14400	0.80	4.5
2	30.07.2016 22:53	-1080	281.49	5.6	73968.5	-6.95	64692.5	-3.57	49400	0.00	16.5	48000	0.25	16.0
3	10.08.2016 10:00	1000	314.92	5.1	25686.3	0.93	12980.3	4.07	19400	2.80	6.0	22800	2.05	6.5
4	12.08.2016 22:01	-1468	285.27	5.5	34001.1	-1.48	29930.8	0.13	29200	0.50	10.5	19000	3.10	9.0
5	27.08.2016 20:58	-1532	295.59	5.8	68949.3	-8.76	51850.6	-5.04	29200	1.35	8.0	21600	3.15	6.5
6	04.09.2016 07:09	-1040	224.33	5.3	35130.5	6.68	-9944.45	18.55	25000	10.00	16.0	41000	6.95	19.5
7	26.09.2016 14:09	-1285	336.66	5.5	37170.7	-4.23	31656.6	-3.07	19400	0.10	5.0	12200	1.80	4.0
8	12.10.2016 10:25	-1268	365.40	5.5	25812.6	3.73	22138.3	5.12	21400	5.15	11.5	17200	5.80	11.0
9	28.11.2016 09:21	-1496	394.49	5.6	5922.9	5.81	12672.4	4.42	13600	4.05	8.0	21400	2.65	8.5
10	11.12.2016 01:20	-1311	276.77	5.3	33226.4	7.04	17223.6	10.75	23800	9.95	17.5	47600	5.60	22.0
11	03.01.2017 18:50	-1130	422.58	5.2	25339.5	-0.53	23871.4	-0.17	21200	0.35	4.0	19800	0.60	4.0
12	12.01.2017 20:12	-1329	410.89	5.3	78516.2	-1.41	54308.1	6.11	77600	0.00	21.5	74200	0.00	22.0
13	31.01.2017 00:10	-1286	323.78	5.4	20961.9	3.02	15379.4	4.54	16800	4.40	9.0	23000	3.05	9.5
14	09.02.2017 09:43	-1306	422.95	5.7	10280.8	3.38	5323.09	4.36	10000	3.50	7.5	10000	3.50	7.5
15	10.03.2017 14:55	-1278	357.56	4.6	3669.0	4.93	11457.2	3.34	10000	3.50	5.0	10000	3.65	5.0
16	01.04.2017 17:55	-1286	276.71	4.8	14622.4	2.67	12871.7	3.17	12000	3.60	6.5	12600	3.45	6.5
17	24.04.2017 13:53	-1323	340.94	4.2	21806.7	5.15	20142.7	5.91	19800	5.95	11.5	27000	4.65	12.5
18	02.05.2017 09:49	-1292	346.78	5	32662.6	0.37	32586.8	0.43	21600	3.25	7.0	17600	4.05	6.5
19	12.05.2017 17:15	1000	322.21	4.8	52576.6	1.19	41109.8	5.90	55000	1.70	23.0	62000	0.90	24.5
20	19.05.2017 17:48	-1237	324.16	4.8	41820.4	-2.94	28353.1	0.96	24800	1.55	10.0	21200	2.25	9.5
21	26.05.2017 09:32	-1030	318.83	5	57171.4	-8.21	35981.4	-2.75	24400	0.20	7.0	13600	2.80	5.5
22	13.07.2017 17:20	1000	358.96	4.9	28927.3	-1.40	21714.5	0.85	25200	0.00	8.0	22000	0.55	8.0
23	21.08.2017 08:50	-1252	309.85	5.2	28464.3	1.73	29753.2	1.27	27000	2.45	8.0	28200	2.20	8.0
24	16.09.2017 17:46	-1221	281.84	5.2	33864.9	-3.44	28567.8	-1.76	19400	0.75	8.0	13200	2.40	7.0
25	30.09.2017 01:37	-1257	253.33	5.2	38622.1	1.17	39850.2	0.13	28200	4.60	11.0	20400	6.55	9.5
26	02.10.2017 23:35	-1490	287.40	5	20987.7	2.42	4785.43	8.09	16800	4.05	14.0	12800	5.10	13.5
27	04.11.2017 16:29	-1800	307.00	5.2	41919.4	-3.24	30796.1	-0.38	24800	1.25	9.0	15000	3.60	7.5
28	10.11.2017 03:38	-1040	274.74	5	35993.8	-2.35	32097.9	-0.63	26600	1.20	10.0	20800	2.75	9.0
29	29.01.2018 10:12	-1280	273.49	4.5	35646.0	3.49	10204.4	13.20	37600	4.10	25.0	30600	4.75	25.0
30	29.01.2018 02:21	-1223	408.87	4.7	17232.5	3.87	15014.5	3.97	11000	5.25	6.5	13400	4.80	7.0
31	02.02.2018 19:09	-1263	411.98	5.3	55992.6	-3.83	35817.2	0.64	36200	0.00	11.0	26600	1.75	10.0
32	01.06.2018 11:03	1000	347.01	4.9	7955.1	4.91	12073.7	4.66	17000	2.75	12.0	18200	2.60	12.0
33	04.06.2018 02:13	-1124	228.13	5.4	22217.2	4.12	3769.18	10.13	11600	7.70	7.5	19800	5.60	8.5
34	09.06.2018 21:24	-1016	282.74	5.4	39786.4	-2.66	48673.1	-4.94	31800	0.00	9.0	31000	0.00	9.0
35	23.07.2018 14:19	-1008	360.78	4.8	22270.7	1.28	10269.8	4.16	14400	3.35	8.5	19200	2.40	9.0
36	04.09.2018 05:15	-1122	259.32	5.6	47993.3	-0.15	67847	-6.68	38400	3.20	11.0	36000	3.65	10.5
37	18.09.2018 12:09	-1266	361.28	4.6	40252.1	6.03	29289.2	8.58	40200	6.60	18.5	37600	6.90	18.0
38	06.10.2018 01:01	-1492	253.36	5.3	17933.2	1.57	24841.8	-0.66	16400	2.10	6.5	12600	3.25	6.0
39	13.10.2018 01:01	-1421	251.36	4.8	16272.6	0.68	14415.6	1.56	13200	2.05	7.5	18800	0.20	8.5
40	17.10.2018 14:47	-1280	345.21	5.2	17102.0	4.57	8681.75	6.32	12000	5.75	8.0	19200	4.50	9.0
41	01.01.2019 16:53	-1540	290.84	4.4	91527.5	-12.44	42393.6	-0.74	27800	3.55	10.5	10000	8.25	7.5
42	16.03.2019 15:18	-1286	305.75	4	89688.2	9.98	-386923	137.73	10000	7.65	25.0	10000	8.25	25.0
43	21.03.2019 10:34	-1307	374.57	4.6	37184.7	0.73	29274.8	2.71	28400	3.20	8.5	30000	2.95	8.5
44	01.04.2019 20:35	-1280	351.46	5.6	70708.9	-11.20	5627.06	6.25	10000	4.90	11.0	11400	5.10	10.5
45	18.04.2019 19:00	-1220	325.80	5.2	-70914.1	-3.03	-105231	7.37	100000	10.00	25.0	10000	10.00	25.0

Event information					RoCof zero crossing method		Fix supporting points method		Optimal fit method with 30s interval			Optimal fit method with 20s interval		
Nr.	Timestamp in CET/CEST	ΔP in MW	P_{Sys} in GW	H_{Sys} in s	K_{FCR} in MW/Hz	k_{SRE} in %/Hz	K_{FCR} in MW/Hz	k_{SRE} in %/Hz	K_{FCR} in MW/Hz	k_{SRE} in %/Hz	H_{Sys} in s	K_{FCR} in MW/Hz	k_{SRE} in %/Hz	H_{Sys} in s
46	24.04.2019 18:09	-1100	326.53	4.4	21376.0	8.92	9674.19	10.80	11800	10.00	15.0	34200	6.10	17.5
47	27.04.2019 02:04	-1296	242.39	4.9	24492.7	0.89	18501.8	2.68	16000	3.50	10.0	22400	1.70	11.0
48	12.05.2019 02:15	-1100	231.40	4.6	501179.0	-78.84	40153.9	27.95	32200	10.00	25.0	10000	10.00	25.0
49	31.05.2019 15:20	955	312.94	4.7	57237.9	-8.31	28146.4	-1.12	22400	0.00	8.0	15600	1.45	7.0
50	01.07.2019 09:27	1026	359.01	5.1	189908.0	-29.35	34924.3	0.20	25600	2.30	9.5	34800	0.50	10.5
51	03.07.2019 12:50	-1038	377.28	4.6	47159.7	-2.33	54904.7	-3.50	37800	0.00	7.5	34000	0.65	7.0
52	25.08.2019 04:19	-1470	216.83	5.5	21860.8	3.38	26982.5	1.06	19800	4.10	9.5	15600	5.50	8.5
53	28.12.2019 07:46	-1220	271.29	5.4	15974.2	2.37	13164.2	3.21	14000	3.05	6.5	16600	2.25	7.0
54	03.03.2020 06:54	-1276	332.90	5	19217.2	-1.10	19725.6	-1.28	14200	0.20	4.0	12400	0.65	4.0
55	18.03.2020 07:10	-1300	316.19	4.9	38343.2	8.17	23529.9	10.39	36000	9.80	20.0	64200	5.85	25.0
56	08.04.2020 14:08	-1168	286.71	4.3	12319.3	4.64	21773.2	2.40	11000	5.40	6.0	10000	5.55	6.0
57	22.04.2020 06:28	-1276	253.54	4.6	22785.0	5.47	13366.3	8.01	18200	6.80	5.5	16400	7.30	5.0
58	08.07.2020 13:07	-1203	351.48	4.7	12235.7	0.51	12963.7	0.27	11400	0.75	4.5	12400	0.55	4.5
59	26.07.2020 01:54	-1050	229.39	5.2	57893.9	2.02	66420.4	2.46	49600	6.95	25.0	37600	8.85	23.0
60	31.08.2020 15:15	-1274	332.24	5	28549.0	-0.74	3512.26	7.20	26600	0.00	15.0	10000	2.80	16.0
61	10.09.2020 11:11	-1400	347.20	4.8	129130.0	-3.95	143656	-5.84	90400	2.10	25.0	84400	3.20	25.0
62	27.11.2020 10:20	-1336	396.27	5.7	31194.9	0.51	24355.2	2.11	27600	1.70	8.5	27800	1.65	8.5
63	30.01.2021 14:57	-1250	334.52	4.7	32648.8	3.81	20815.8	7.85	15800	9.05	14.0	10000	9.35	13.0
64	17.05.2021 16:34	-3500	317.48	4.2	25751.8	0.90	20773.5	2.24	15000	3.95	8.0	10000	5.10	7.5

Eidesstattliche Erklärung

Hiermit erkläre ich, dass die vorliegende Arbeit gemäß dem Code of Conduct, insbesondere ohne unzulässige Hilfe Dritter und ohne Benutzung anderer als der angegebenen Hilfsmittel, angefertigt wurde. Die aus anderen Quellen direkt oder indirekt übernommenen Daten und Konzepte sind unter Angabe der Quelle gekennzeichnet.

Die Arbeit wurde bisher weder im In- noch im Ausland in gleicher oder in ähnlicher Form in anderen Prüfungsverfahren vorgelegt.

Elias Obererlacher

Ort, Datum

Unterschrift